Performance studies of data acquisition for the GAINS spectrometer at the GELINA accelerator facility

Tatiana D'Agostini Herstad
EES-2021-490

Master Programme Energy and
Environmental Sciences, University of Groningen

university of groningen / faculty of science and engineering / energy and sustainability research institute groningen

Research report of Tatiana D'Agostini Herstad

Report: EES-2021-490

Supervised by:
Dr. Myroslav Kavatsyuk, Nuclear Energy

University of Groningen
Energy and Sustainability Research Institute Groningen, ESRIG

Nijenborgh 6
9747 AG Groningen
T: 050 - 363 4760
W: www.rug.nl/research/esrig

TABLE OF CONTENTS

SUMMARY

As the world moves towards more sustainable energy sources, a renewed interest in nuclear energy has emerged. An important aspect of studies in the field are neutron cross-section studies. The GAINS experiment at the GELINA neutron time-of-flight facility aims to do just that. This experiment makes use of a digitizer for data processing.

The present research studies the performance of said digitizer. To do so, the dead time, the energy, and the time resolution of the digitizer are investigated. An emphasis is placed on the feasibility of achieving the resolution nuclear data requires while decreasing the amount of data stored.

The digitizer includes software that allows for data filtering before collection. Further processing is done online. Two different detectors with different technical specifications are used to improve resolution and investigate the digitizer's behavior. A ^{22}Na source is used, and the energy resolution is compared to that achieved in previous studies on the 511 keV peak of this isotope. The timing resolution is compared to that achieved in literature by the respective detectors, and the suitability of this kind of data acquisition and processing is determined.

LIST OF ABBREVIATIONS

FWHM: Full-Width at Half-Maximum

G: Gap time

GAINS: Gamma Array for Inelastic Neutron Scattering

GELINA: Geel Electron Linear Accelerator

HPGe: High-Purity Germanium

LYSO: Lutetium Yttrium Oxyorthosilicate

MAW: Moving Average Window

P: Peaking time

1. INTRODUCTION

As we move away from fossil fuels, there is a need for alternative sources of energy. Nuclear energy has long been an interesting option with many advantages, but that has been marked by events such as the Chernobyl and Fukushima accidents. As a result, public acceptance of this energy source has decreased, resulting in many countries opting out or decreasing this source's share in the energy mix (Bauer, Gylstorff, Madsen, & Mejlgaard, 2019). But as the climate crisis worsens, nuclear energy is once more gaining popularity.

When conducting research on nuclear energy, one of the most important aspects to investigate is the neutron cross-section. Accurate measurements of this quantity are necessary for the development of new nuclear reactors, such as Generation IV reactors, and the improvement of safety features (Boromiza, et al., 2020; Mihailescu, Olah, Borcea, & Plompen, 2004). In particular, inelastic scattering, as the main energy loss mechanism for fast neutrons, is of special interest (Pirovano, et al., 2017).

Studying these neutron interactions and cross-sections is the purpose of the Gamma Array for Inelastic Neutron Scattering (GAINS) spectrometer at the Geel Electron Linear Accelerator (GELINA) facility in Belgium (Rouki, 2012).

GELINA is a neutron time-of-flight facility that counts on several paths which allow for simultaneous conduction of up to 12 experiments. The facility consists of a linear accelerator with a Uranium target, which acts as a neutron source for the experiments (European Commission, 2020). At GELINA, the GAINS experiment is set up at 200 m flight path from the white neutron source. As an electron beam hits the Uranium target, it produces bremsstrahlung radiation. In turn, this reacts with the target through (γ, n) and (γ, fission) reactions occur, releasing neutrons (Boromiza, et al., 2020; Negret, et al., 2007). These are later scattered from a sample, producing gamma rays which are then detected by the spectrometer consisting of 12 high purity Germanium (HPGe) detectors (Mihailescu, Olah, Borcea, & Plompen, 2004; Kerveno, et al., 2015). The obtained data is subsequently analyzed by a digitizer.

Using the time difference between the generation of neutrons at the source and the detected gamma rays, the velocity and thus energy of the neutrons can be obtained (Rouki, 2012). Additionally, the energy data can be used to identify and construct energy levels and transitions (Mihailescu, Olah, Borcea, & Plompen, 2004; Kerveno, et al., 2015). This calls for equipment with exceptional energy and time resolution.

Furthermore, nuclear data is notably large and should be of high quality. Researchers are often restricted by the resolution and processing power of the equipment used. This limits the number of events that can be processed per unit time and thus the quality of the data. For this purpose, the amount of data to be processed should be diminished by making use of resources made available by the digitizer’s software. These include applying filters and only requiring the necessary data. This allows the storage of only energy and time data instead of that of entire waveforms.

2. RESEARCH AIM

The aim of this research is to investigate the performance of the data acquisition systems for this setup with the goal of achieving good time and energy resolution. This will be done with a focus on the feasibility of achieving the necessary data acquisition and analysis standards while requiring minimal data.

2.1 Research Questions

The research question is:

- What resolution can be achieved with the digitizer and algorithms?

There are several sources of error in the obtained data. Most notably, noise can diminish the quality of the data, but there is also a resolution that is intrinsic to the digitizer and cannot be improved upon by algorithms. Therefore, the research question will be explored through different angles.

2.1.1 Dead time

The digitizer has an inherent dead time that is a result of the time it spends processing the events. During this time, no events that occur can be detected. The resulting dead time is the sum of the bank swap dead time and the hit/event storage dead time (SIS GmbH, 2020).

The digitizer contains two banks, or memories, where events are recorded and processed. After one has been filled, the digitizer swaps to the second bank so that more events can be detected while the first bank finishes processing. However, this swapping takes some time during which no events are recorded, which is the bank swap time (SIS GmbH, 2020). In addition, there can be a so-called swap event active time contributing to the bank swap dead time. This value depends on the active time and on the moment of the swap when a bank is still trying to save an event, and ranges from 0 to the event active time (SIS GmbH, 2020).

The event active time is the sum of the event length, or active trigger gate window length, plus the hit/event dead time.

The hit/event dead time is simply the time that has passed between the moment an event has ended and the moment the software is ready to take up a new event. This is the sum of the time it takes to end the event, the time it takes to save the test data, and the time it takes to save the calculated values, such as energy values. The latter depends on which values are chosen (SIS GmbH, 2020).

The resulting dead time can be calculated the following way:

$$Dead\ time = t_{BankSwap} + t_{SwapEventActive} + t_{End} + t_{SaveMAWTestData} + t_{SaveCalculateValues}$$

The event active time is:

$$t_{EventActive} = t_{ActiveTriggerGate} + t_{End} + t_{SaveMAWTestData} + t_{SaveCalculateValues}$$

For a sample clock of 250 MHz, $t_{BankSwap}$ is constant at 144 ns.

In this research, the maximum length of the event is about 1000, which corresponds to 4 µs; the length of the sample was chosen to be 1000, and the MAW sample length taken was 0. The software was asked to save energy data, and only channel 1 was active. These settings correspond to the following values:

$$t_{End} = 250 - 470\ ns$$

$$t_{SaveMAWTestData} = 0$$

$$t_{SaveCalculateValues} = 76\ ns$$

The event active time is then:

$$t_{EventActive} = 4\ \mu s + (250, 470)\ ns + 76\ ns = 4.33 \text{ to } 4.55\ \mu s$$

This means that $t_{SwapEventActive}$ could be anywhere from 0 to 4.55 µs, and therefore the total dead time is:

$$Dead\ time_{1000} = 144\ ns + (0, 4550)\ ns + (250, 470)\ ns + 0 + 76\ ns = 0.47 \text{ to } 5.2\ \mu s$$

Other settings explored in this research are an event length of 500 and a length of the sample of 500, an event length and length of the sample of 100. These settings only change the event active time into 2.33 to 2.55 µs and 0.75 to 0.946 µs respectively. This translates to the following dead times:

$$Dead\ time_{500} = 144\ ns + (0, 2550)\ ns + (250, 470)\ ns + 0 + 76\ ns = 0.47 \text{ to } 3.24\ \mu s$$

$$Dead\ time_{100} = 144\ ns + (0, 946)\ ns + (250, 470)\ ns + 0 + 76\ ns = 0.47 \text{ to } 1.64\ \mu s$$

This prompts the first sub-question:

- What is the dead time of the digitizer, and what effect does sample length have on said dead time?

2.1.2 Energy resolution

To measure the energy spectrum of a certain isotope, particle detectors are used. Two popular types are scintillating detectors and semiconductor detectors. HPGe detectors fall into the latter category, while LYSO detectors, which will also be used in this research, fall into the former.

Scintillating detectors contain a scintillating material, which absorbs the incoming particle and produces photons of the same energy. These then enter a photomultiplier tube, which converts the photons to electrons, multiplies them, and produces a current (Kramar, 2017).

Semiconductor detectors make use of two oppositely doped semiconductors separated by a depletion region. In this region, the charges of the two semiconductors recombine, resulting in a zone devoid of free charge carriers. This is known as a p-n junction diode, which is connected to a circuit. When a particle hits the depletion region, electron-hole pairs are produced, which create a potential difference in the circuit and produce a current (Lutz & Klanner, 2020).

In both cases, the produced currents are associated to the energies of the incoming particle, making it possible to trace back the initial particle through the observed energy spectrum. As an atom decays, then, this should lead to a delta function corresponding to the energy of the particle released by the decay. Subsequent processes the atom and its daughter particles may endure should also result in a delta function.

In reality, there is some statistical variation between the number of charge carriers produced (Lecoq, 2020). The resulting shape is a Gaussian distribution. The width of this Gaussian distribution gives the energy resolution of the setup; the narrower the peak, the better the resolution. The energy resolution is defined as an instrument's ability to distinguish between gamma rays close in energy (Daube-Witherspoon, 2014).

The energy resolution of HPGe detectors is significantly better than that of LYSO detectors. For the 511 keV peak of ^{22}Na, HPGe detectors have a gamma energy resolution of 2.58 keV FWHM, whereas for LYSO detectors this resolution is about 59.28 keV FWHM (Alkhorayef, Alzimami, Alfuraih, Alnafea, & Spyrou, 2012; Beltrame, et al., 2011). This means that HPGe detectors are significantly better at differentiating energy pulses.

However, HPGe detectors also have disadvantages, such as the need to be cooled by liquid nitrogen, making them less versatile (Abuelhia, Alzimami, Alkhorayef, Podolyak, & Spyrou, 2008). Furthermore, the detector's timing resolution is not stellar without optimization and is

often outperformed by scintillating detectors (Gladen, et al., 2020; Abuelhia, Alzimami, Alkhorayef, Podolyak, & Spyrou, 2008; Crespi, et al., 2010).

But the digitizer has a certain resolution as well. The achieved resolution will reflect both the digitizer's and the detector's resolution. Considering this, the following sub-question is posed:

- What energy resolution can be achieved by making use of the digitizer?

2.1.3 Time resolution

Time resolution depends on the rise time and the height of the pulse. Scintillators have particularly good rise and response times, making them the most suitable type for measurements concerning time resolution (van Eijk, 2014).

The time resolution of HPGe detectors is limited to a few tens of nanoseconds. Electric noise and a rise time that depends on the position of the gamma interactions are responsible for this. However, further analysis and event selection can improve this, achieving coincidence resolutions in the order of 4 ns (Crespi, et al., 2010; Gladen, et al., 2020).

Conversely, the coincidence time resolution of LYSO detectors is in the order of a few hundred picoseconds, dropping below 200 ps in some studies (Auffray, et al., 2013; Jun-Hui, et al., 2015; Doroud, Williams, Zichichi, & Zuyeuski, 2015). Plastic scintillators provide even better time resolution, with some reaching values as low as 5 ps (Zhao, et al., 2016).

Just as with the energy resolution, the achieved time resolution will be a product of the detector's and the digitizer's resolution.

This brings up the last sub-question:

- What time resolution can be achieved with the current setup?

3. METHOD

3.1 The digitizer

The digitizer to be studied is Struck's SIS3316 digitizer. Until recently, Acqiris' DC440 digitizer was used for the GAINS experiment, which has a resolution of 12 bit and a sampling rate of 420 MHz (Kerveno, et al., 2015). The SIS3316 has a better resolution at 14 bit but a worse sampling rate at 250 MHz (SIS GmbH, 2020).

The digitizer consists of 16 channels through which an input can be fed. Depending on the setup, only one or two will be occupied in this research.

The digitizer's software allows us to only record certain data, such as a specific number of events or a specific type of data. It also performs some processing on the recorded events, such as implementing energy and trigger filters. The way these work will be explained in the next section.

3.2 Setup

First, the dead time of the digitizer will be studied. This will be done with random pulse generators and the digitizer software. The pulse generators are BNC's tail pulse generator model BH-1 as the first generator, and BNC's random pulse generator model SB-2 as the second. These generators are connected in such a way that the signal in the first generator serves as the trigger for the second one. The second signal is given a delay of a few microseconds with respect to the first one. The signals are then mixed through a dual sum mixer to produce a single signal which is then sent to a single channel in the digitizer. This digitizer is connected to a computer for data processing and storing. The measurements will be supported by an oscilloscope, which will be used to give an estimate on the time difference between pulses.

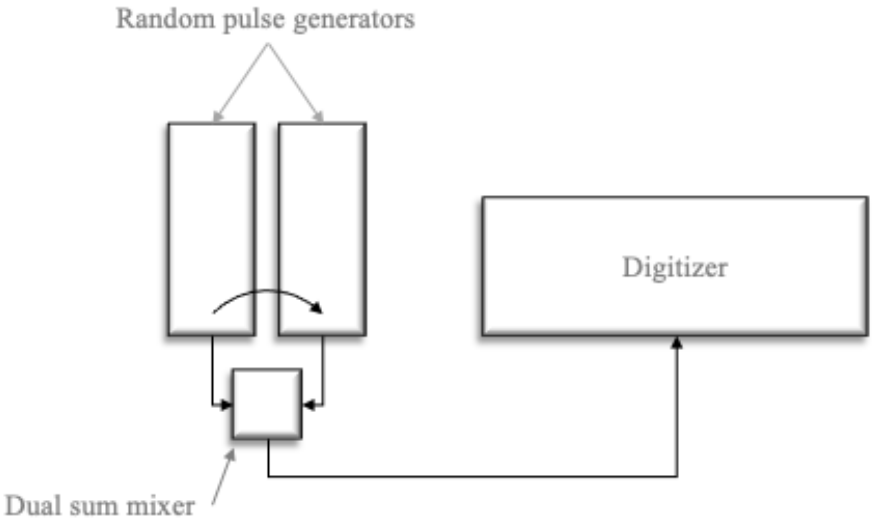

Figure 1: Setup for dead time measurements.

The result of sample length on the digitizer's dead time will be explored. As alluded to earlier, the sample and event lengths used will be 100, 500 and 1000. The obtained dead time will be compared to the theoretical dead time calculated above.

For the energy and time resolution, different setups will be used with different purposes.

First, test results will be obtained by using two identical, diametrically opposed detectors connected to the digitizer. These detectors consist of a LYSO scintillation crystal (see, for

example, Alva-Sanchez, et al., 2018), a preamplifier, and a photosensor, and are fed a voltage. They are connected to two different channels of the digitizer, which is in turn connected to a computer. The detectors are slightly radioactive and interact with one another. Additionally, a radioactive ^{22}Na sample will be placed between the detectors to increase the count rate.

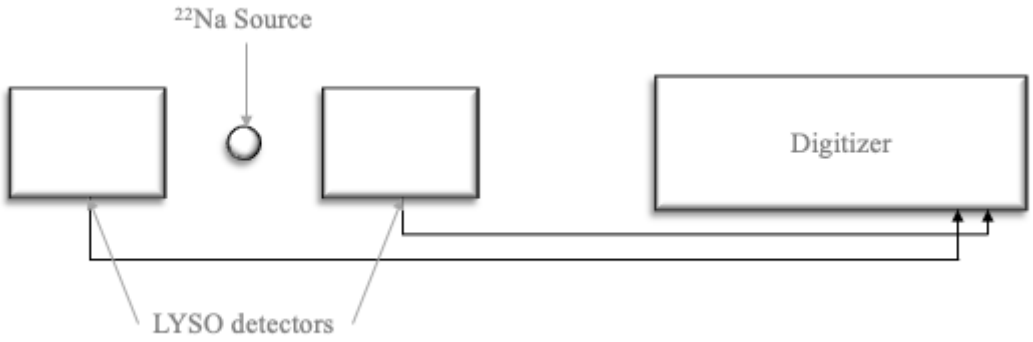

Figure 2: Setup for resolution measurements with scintillating detectors.

The aim of this setup is to get familiarized with the workings of the software and hardware; achieving the best possible resolution is not a priority for these initial results.

Next, more accurate data will be obtained by making use of an HPGe detector. This detector is placed inside a lead container to shield it from external noise.

For the energy resolution, this detector will be connected to the digitizer as the only detector. The ^{22}Na source will be placed above the detector. For the time resolution, one of the scintillating detectors used previously will be connected to a second channel, and the ^{22}Na source will be placed between the detectors. The inclusion of a scintillating detector is an effort to improve the poor time resolution of the HPGe detector.

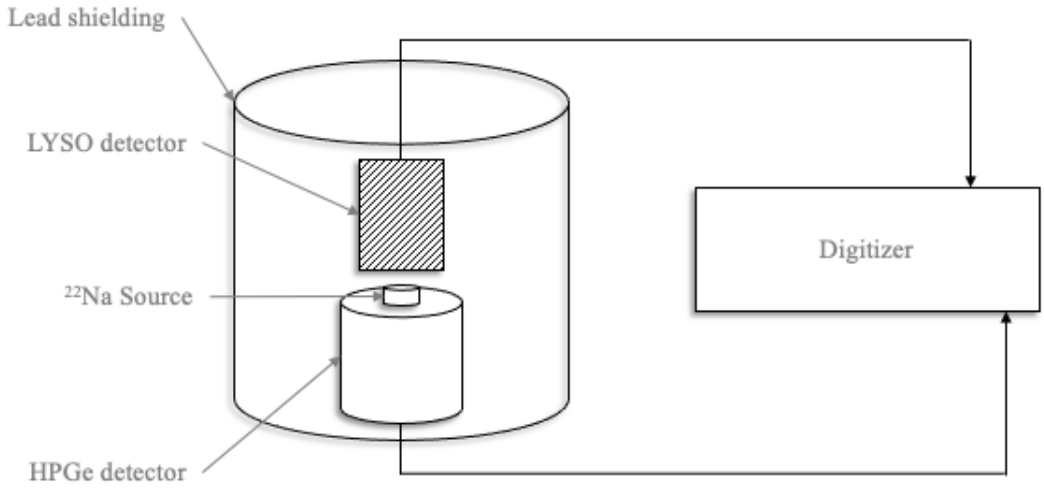

Figure 3: Setup for resolution measurements with a HPGe detector. The scintillating detector is only in place for the time measurements.

The acquired data will be analyzed with a program using a computer.

For both setups, energy and time measurements will be obtained, and the effect of different filter values on resolution will be studied. This will be compared to the resolutions found in literature for each detector to determine the suitability of the digitizer.

3.3 Sodium-22

To investigate the energy and time resolution, Sodium-22 will be used. This isotope decays mainly through β+ decay to Neon-22, emitting positrons and electron neutrinos. These positrons promptly collide with electrons and are then annihilated, producing photons of the same energy as the particles' mass (IAEA, 2021). This is the 511 keV peak observed in Figure 4, and the peak of interest for this research. In most cases, ^{22}Na decays to an excited state of ^{22}Ne, which then drops to the ground state, emitting a photon. This is the 1275 keV peak seen in Figure 4.

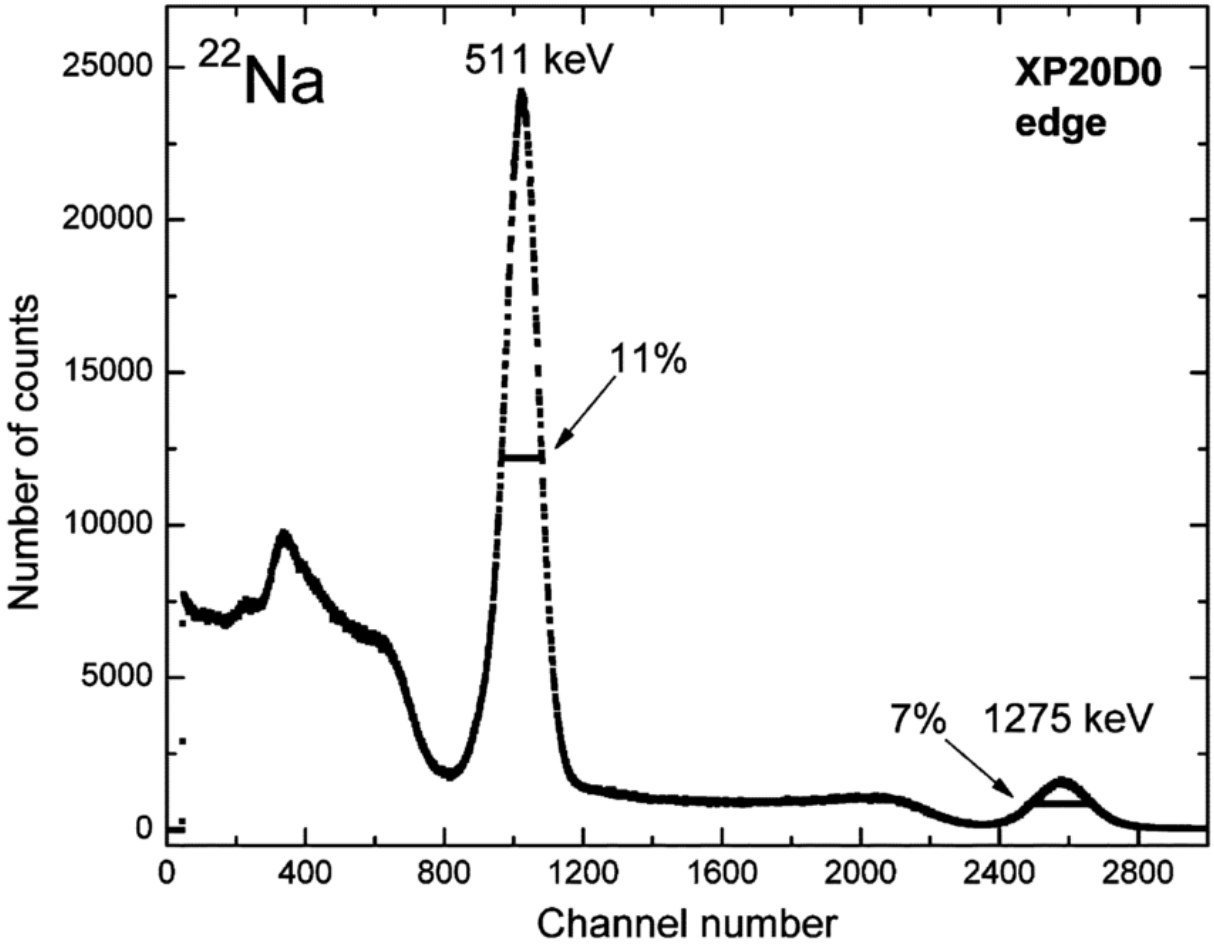

Figure 4. Energy spectrum for ^{22}Na. The percentages shown in the picture correspond to the energy resolution the authors achieved for each of the peaks with an LSO scintillating detector (Moszynski, et al., 2006).

The photons observed as a result of electron-positron annihilation will go in opposite directions, whereas those that were spontaneously emitted will go in all directions. This will have repercussions on the observed spectrum for different setups.

4. DATA ACQUISITION AND PROCESSING

The data is taken in windows of a given length within which an event is sampled. These windows are prompted by trigger pulses that can be internal or external.

When the signal from a pulse generator or from a decay generates a pulse, this triggers the start of the sampling and thus the beginning of the window.

4.1 Processing

As the digitizer records a pulse, it processes it into what is called a moving average window. This is produced by subtracting two points in the pulse, taking an average, and effectively reducing noise. The resulting shape is usually a trapezoid, as seen in Figure 5. The number of points is given by the Peaking time (P), whereas the distance between any two regions to be subtracted is given by the Gap time (G). These two parameters are adjustable. Additionally, a decay correction factor may be necessary to correct for internal decays (SIS GmbH, 2020).

In general, increasing P and G values results in an increase in resolution by decreasing noise. However, the digitizer has an intrinsic resolution that is given by its properties which cannot be improved upon by reducing noise. When this resolution has been reached, P and G can be said to have reached a saturation point. Moreover, larger P and G values also mean more pileups. These are produced whenever two signals overlap. In particular, for neutron studies, photons produced by delayed neutrons could overlap with those produced by fast neutrons from different events, leading to undesirable pileups. To avoid these, the pulse width should be kept relatively small by minimizing P and G (Luo, et al., 2018).

Therefore, there should be optimal P and G values which offer the best possible resolution without compromising the data.

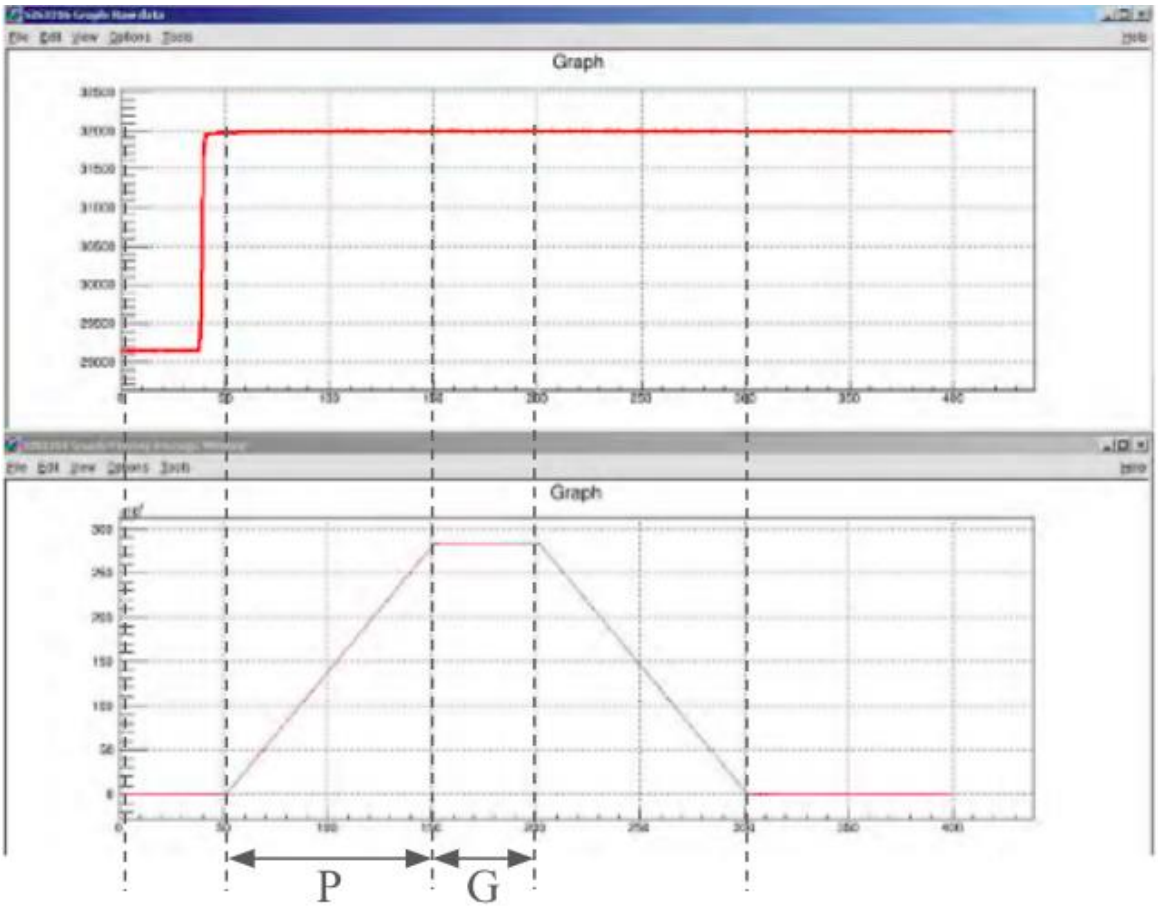

Figure 5. From top to bottom, raw data and moving average window for a step function with P = 100 and G = 50 (SIS GmbH, 2020).

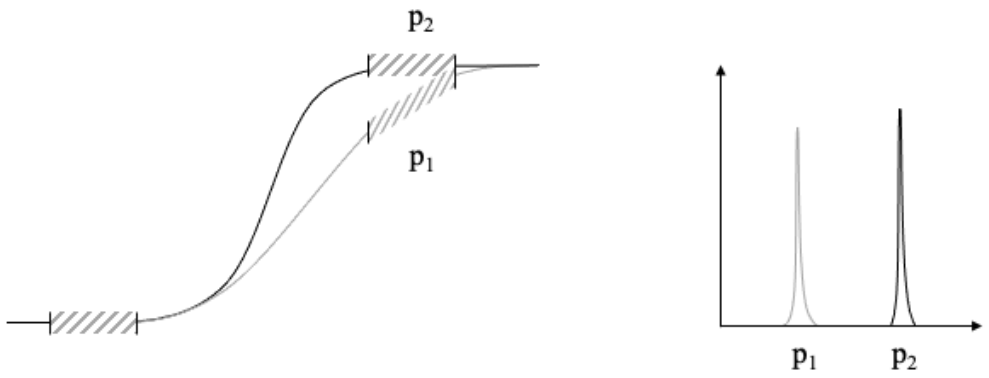

Figure 6: Effect of choosing suboptimal P and G values. Here, p_1 has a longer rise time than p_2, with equal P and G. Because in p_1 the maximal amplitude hasn't been reached, the resulting peak is smaller in amplitude and contains less data than that of p_2.

Figure 5 shows how the moving average window is produced from the raw data, while Figure 6 shows the importance of choosing appropriate P and G values. For energy data, this figure shows that with inappropriate values the maximum energy may not be recorded, leading to worse resolution.

The digitizer's software has energy and time data as outputs. This data is used by a root program to produce an energy and time difference spectrum. This program has been set up to only process data from the digitizer's channels that are used. The different features of this program and of the digitizer's software for each of the research questions will be explained below.

4.2 Dead time

In order to investigate the dead time inherent to the digitizer under the chosen settings, the root program subtracts the timestamps of two consecutive events and records them. This corresponds to the time difference between the two. A histogram is then drawn, allowing us to visualize this difference (Figure 7, top).

If within a single window there are two events, we expect to see two peaks in the histogram, one corresponding to the periodical time difference between events in two different windows and the other to the time difference between events in a single window (Figure 7, bottom).

Therefore, if two separate signals have been sent out but only one peak is shown, this means that the second pulse has fallen within the dead time between windows.

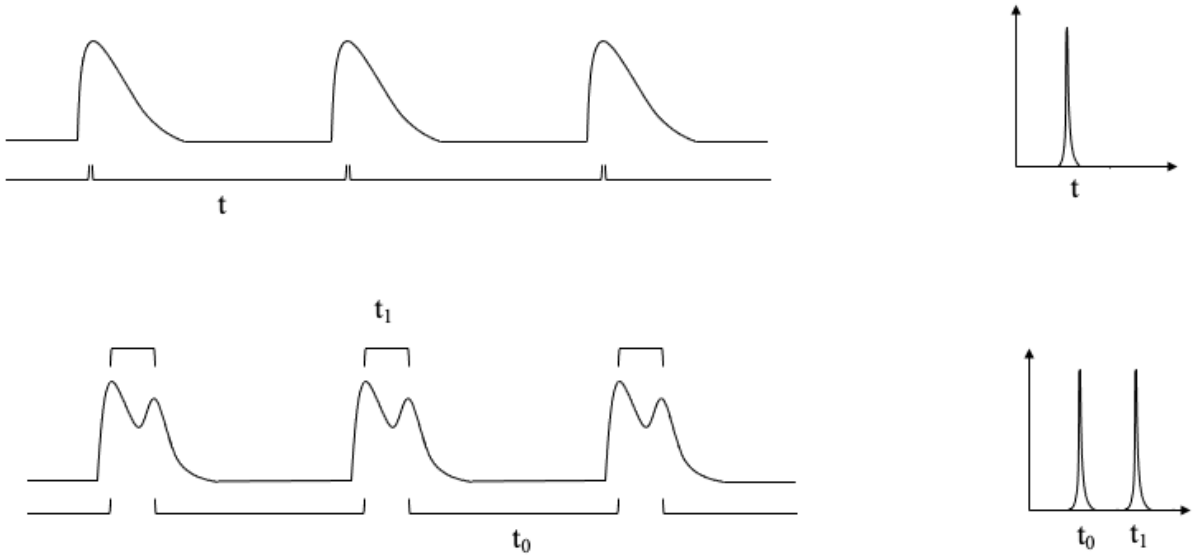

Figure 7: Data collection algorithm for dead time. t and t_1 are the periodical differences between peaks in consecutive windows, whereas t_0 is the difference between consecutive peaks within a single widow.

4.3 Resolution studies

4.3.1 Energy resolution

The energy data is readily provided by the digitizer's software. The root program allows us to apply a gaussian fit on the chosen peak, yielding its maximum value and standard deviation. These values can be used to find the relative energy resolution of the peak. The resolution is given by the width of the peak; a narrower peak reflects better statistics and thus a better resolution. The location and absolute width of the peak will vary with P and G, so by finding the relative energy resolution instead of the absolute, the data can be calibrated and compared to one another to find optimal settings. This is not the case for the time resolution, so absolute values are used then.

For the energy resolution, it is important to minimize background noise by ensuring that the detected particles belong to an event. To do so, the software is set up to look for coincidences for the LYSO detector setup. That is, the program searches for instances when a particle was detected in both detectors at the same time. This is done by both the digitizer's software and the root program.

The energy data can also be used to improve the time resolution by indicating to the root program in what part of the spectrum to look. To do so, the program plots the energy of channel 2 against that of channel 1, allowing us to choose events where photon deposition is present in both channels.

4.3.2 Time resolution

To find the time resolution, the root program finds the difference in timestamps between the two channels, minus a correction, if included. This is then plotted, once again allowing for a gaussian fit and providing statistics.

The time correction is applied to make the result amplitude independent. To obtain this correction, the program looks at three values of the moving average window for better

resolution: the maximum value, the value before the trigger and the value after the trigger. These values are then used to make a linear interpolation to find a negative time offset (SIS GmbH, 2020). The resulting value is shown in Figure 8.

The program also allows us to look solely at the time resolution of the values where photon deposition occurs in both channels, as explained above. This works exactly as the normal time resolution program does, but only analyzes the values within the chosen parameters.

Unlike for the energy resolution, coincidences were not required on the digitizer's software for the time resolution. Preliminary results showed that when looking for coincidences, the resulting time spectrum was a measure of the time difference instead of the timing of the coincidences themselves, yielding results for time resolution that are better than reality. Here, coincidences were only looked at after data acquisition through the root program.

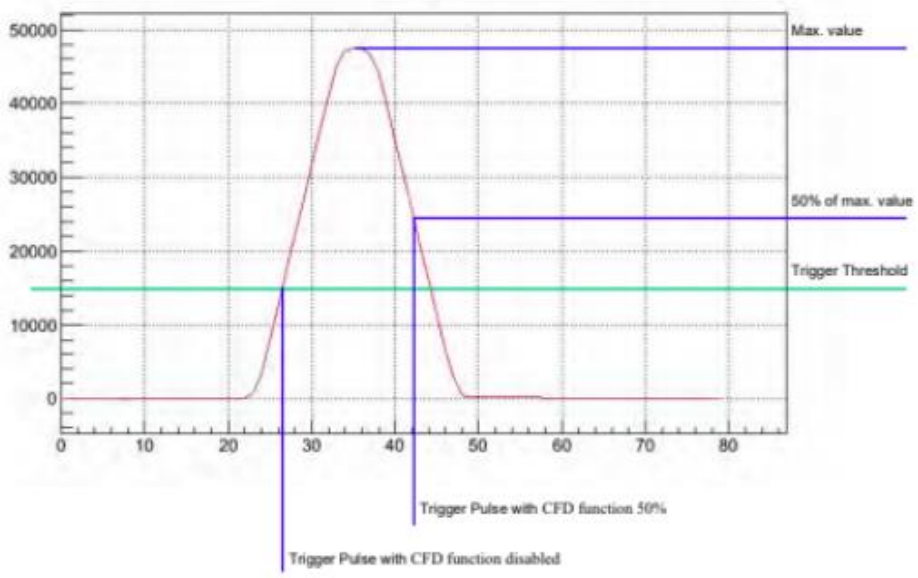

Figure 8: Time correction on the MAW of a step function with P = 10 and G = 4 (SIS GmbH, 2020).

5. RESULTS

5.1 Dead time

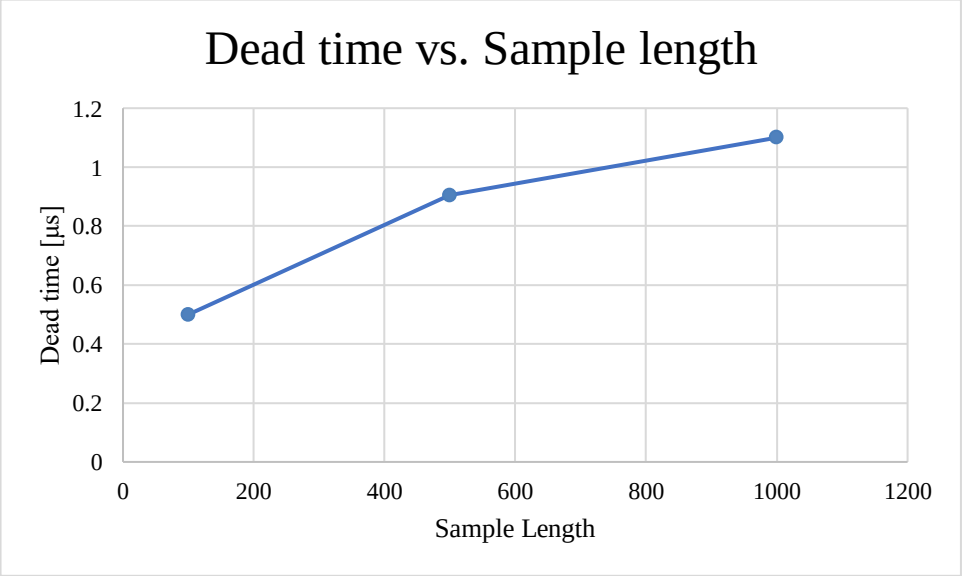

Figure 9: Dead time as a function of sample length.

As expected, the dead time increases with increasing sample length. The obtained dead time falls within the calculated dead time for all sample length values.

5.2 Energy resolution

5.2.1 Scintillating detectors

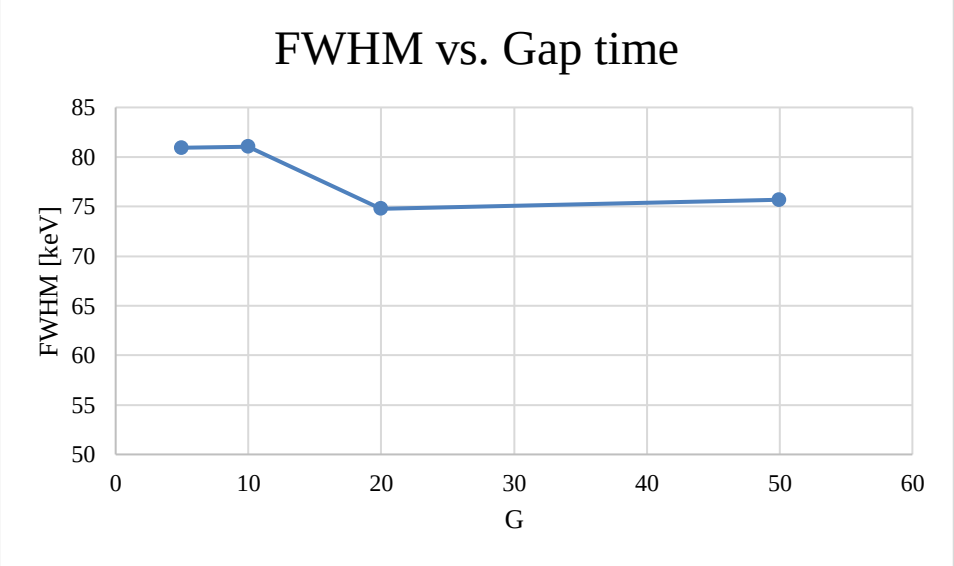

Figure 10: Energy resolution at FWHM for the 511 keV peak vs. Gap time with P = 50 for a LYSO detector.

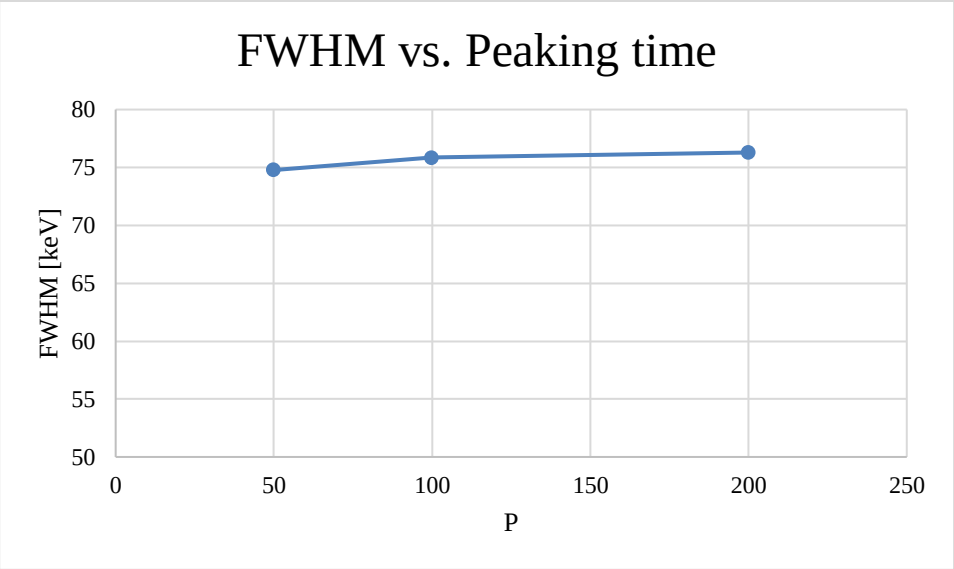

Figure 11: Energy resolution at FWHM for the 511 keV peak vs. Peaking time with G = 20 for a LYSO detector.

The best achieved resolution was 74.77 keV FWHM at P = 50 and G = 20.

Inspecting Figure 11, it is clear that this resolution could probably be improved upon by changing the value of P.

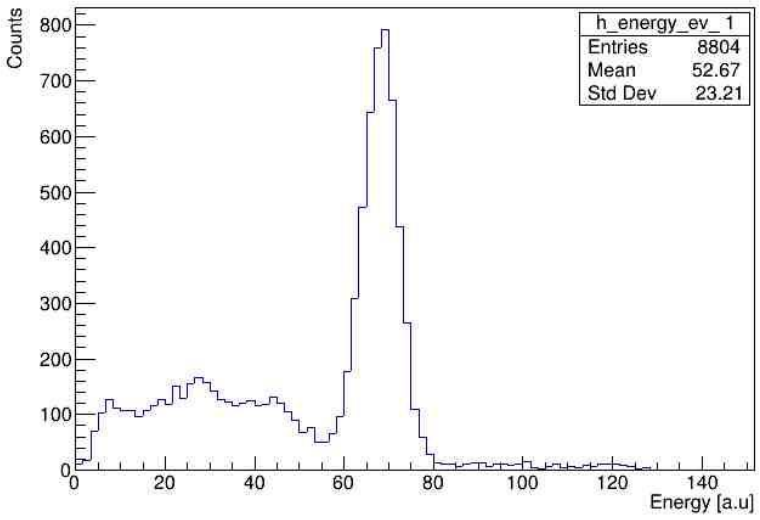

Figure 12: Energy spectrum for ^{22}Na with G = 20 and P = 50 with LYSO detectors.

5.2.2 HPGe detector

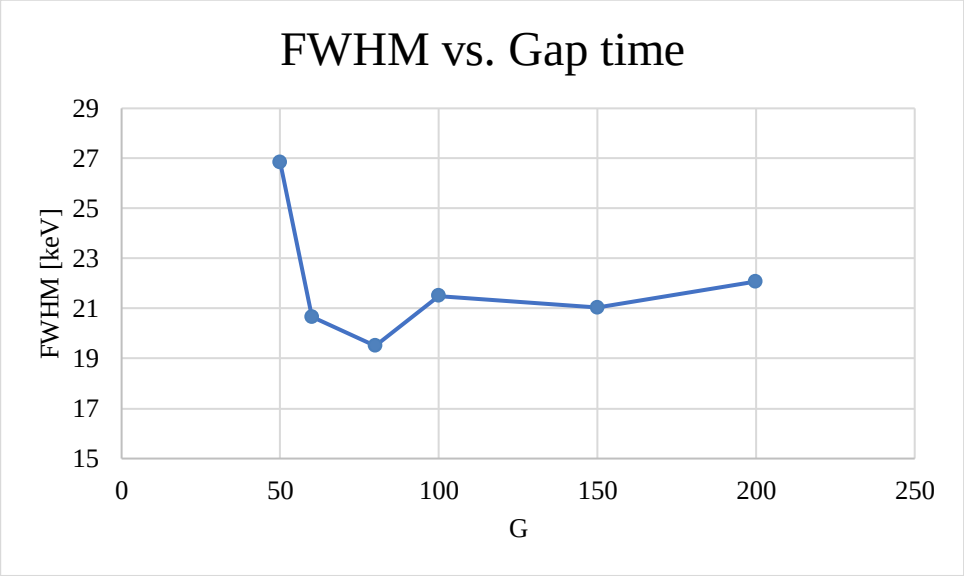

Figure 13: Energy resolution at FWHM for the 511 keV peak vs. Gap time with P = 100 for an HPGe detector.

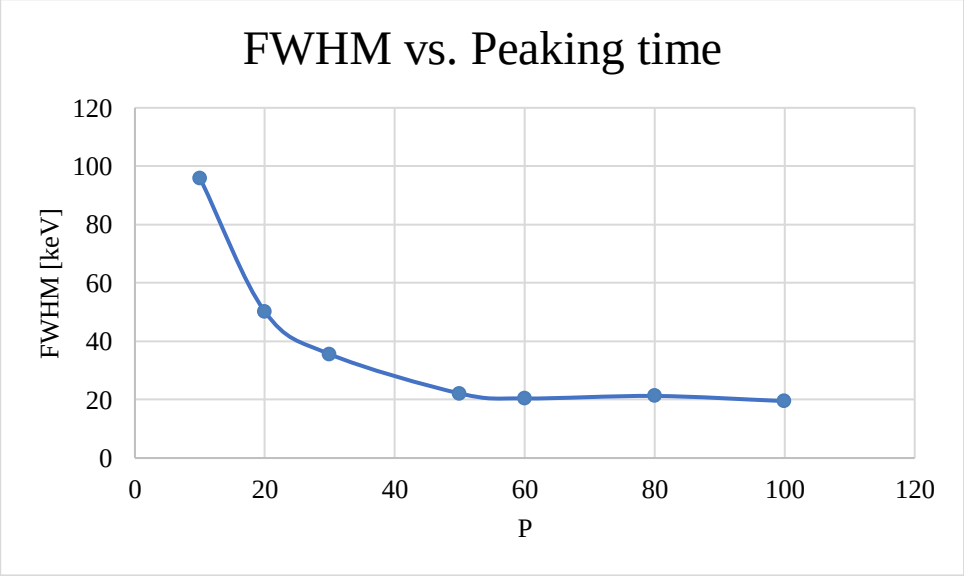

Figure 14: Energy resolution at FWHM for the 511 keV peak vs. Peaking time with G = 80 for an HPGe detector.

The best achieved energy resolution was 19.51 keV FWHM at G = 80 and P = 100.

This is an improvement from the LYSO detectors, but much worse than expected from literature.

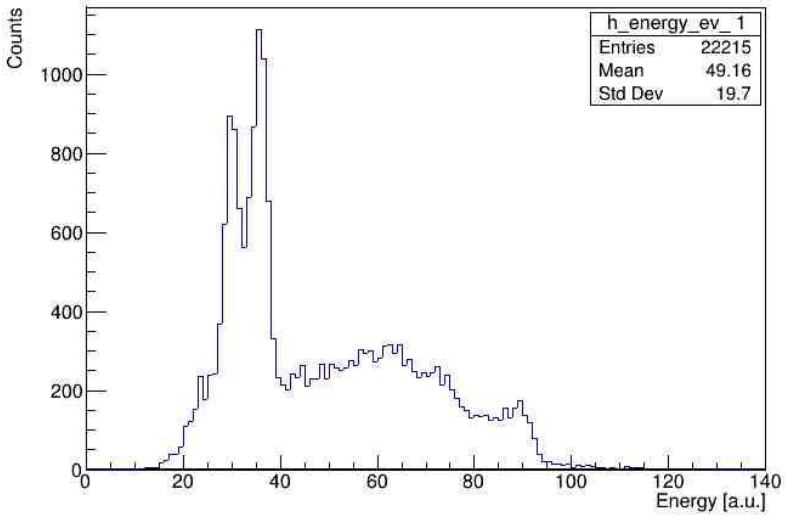

Figure 15: Energy spectrum for ^{22}Na with P = 10 and G = 50 with the HPGe detector. This corresponds to the worst energy resolution obtained.

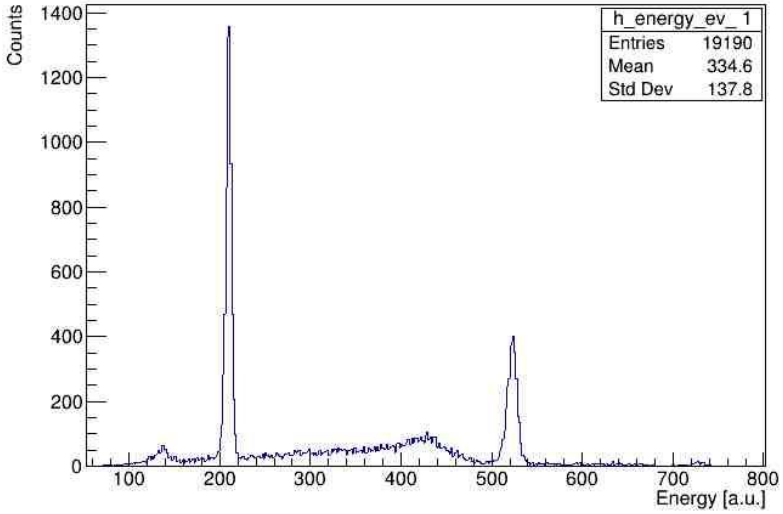

Figure 16: Energy spectrum for ^{22}Na with P = 60 and G = 80 with the HPGe detector.

Figure 16 shows the 511 keV peak on the left and the 1245 peak on the right.

5.3 Time resolution

5.3.1 Scintillating detectors

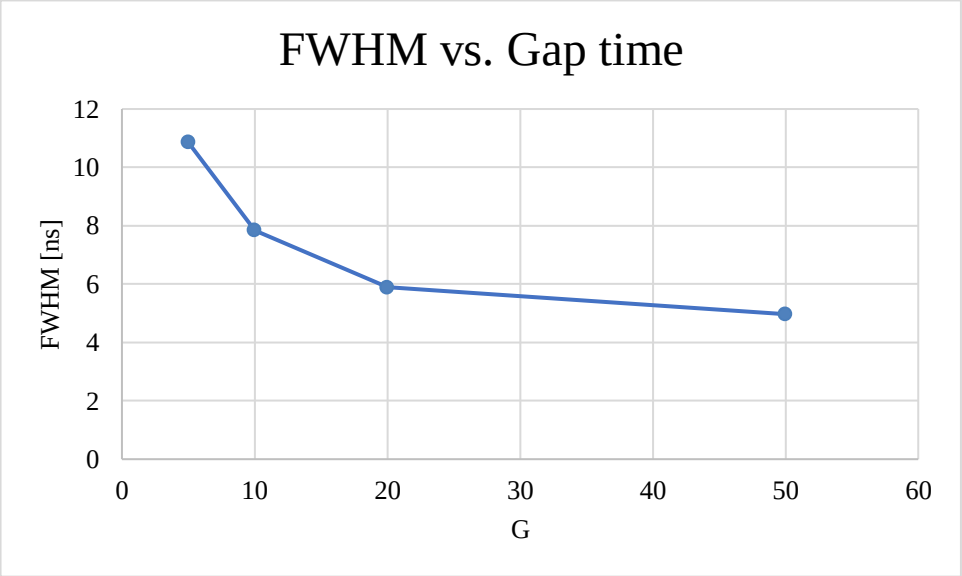

Figure 17: Time resolution at FWHM vs. Gap time at P = 4 for LYSO detectors.

The time resolution of the plotted time difference was found to decrease with increasing Gap time, which translated into better time resolution. The lowest value of the time resolution was found to be 4.97 ns at FWHM at G = 50.

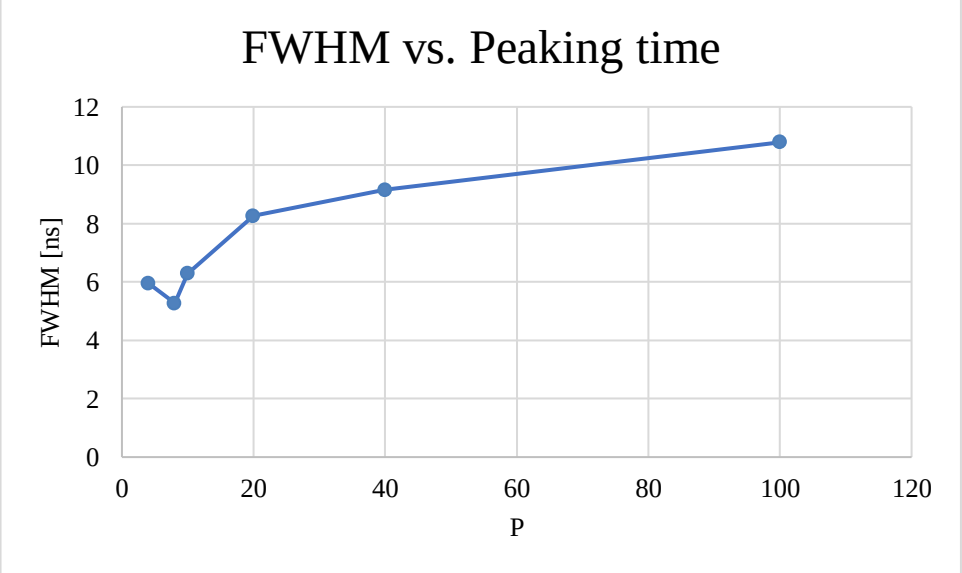

Figure 18: Time resolution at FWHM vs. Peaking time at G = 20 for LYSO detectors.

The time resolution dips at P = 8 before increasing with increasing values of P. Therefore, for G = 20 the best achievable resolution is 5.28 ns at FWHM at P = 8.

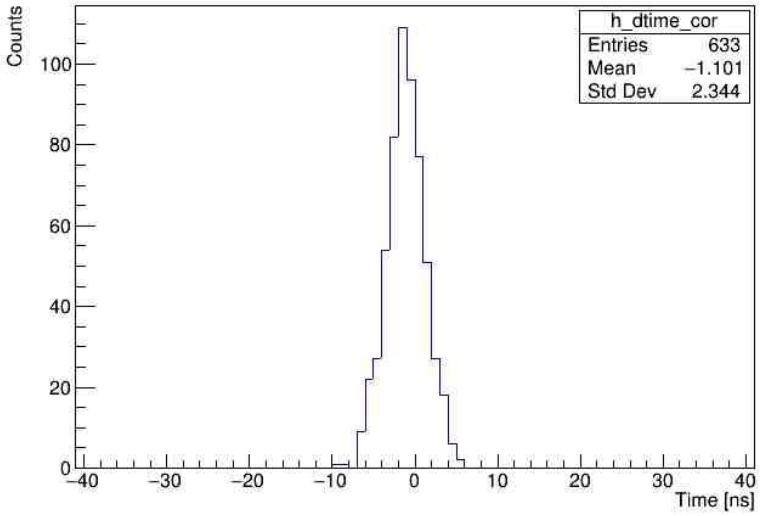

Figure 19: Time resolution for LYSO detectors with P = 8 and G = 20.

5.3.2 HPGe detector

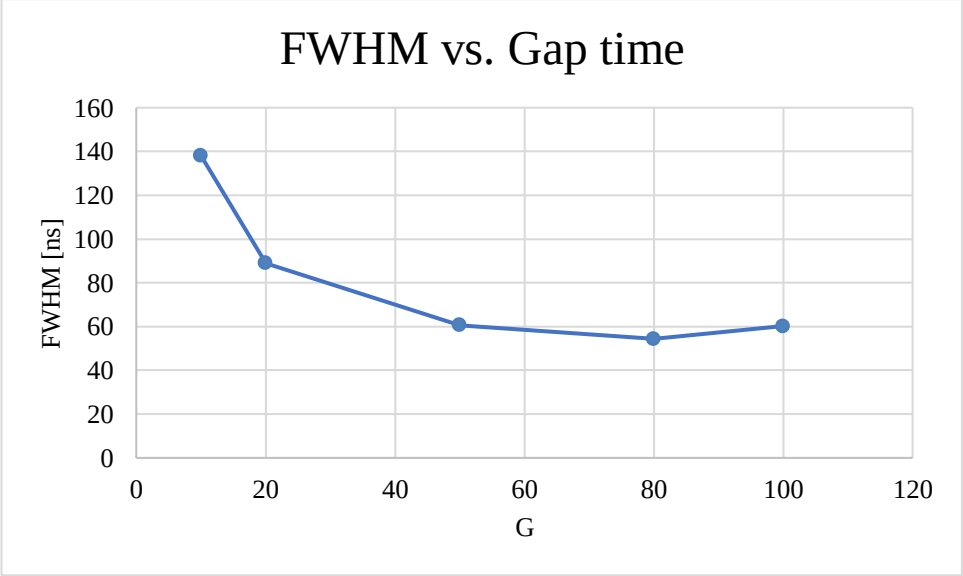

Figure 20: Time resolution at FWHM vs. Gap time at P = 4 for HPGe and LYSO detectors.

For P = 4, the best time resolution is achieved at G = 80 with a value of 54.40 ns at FWHM.

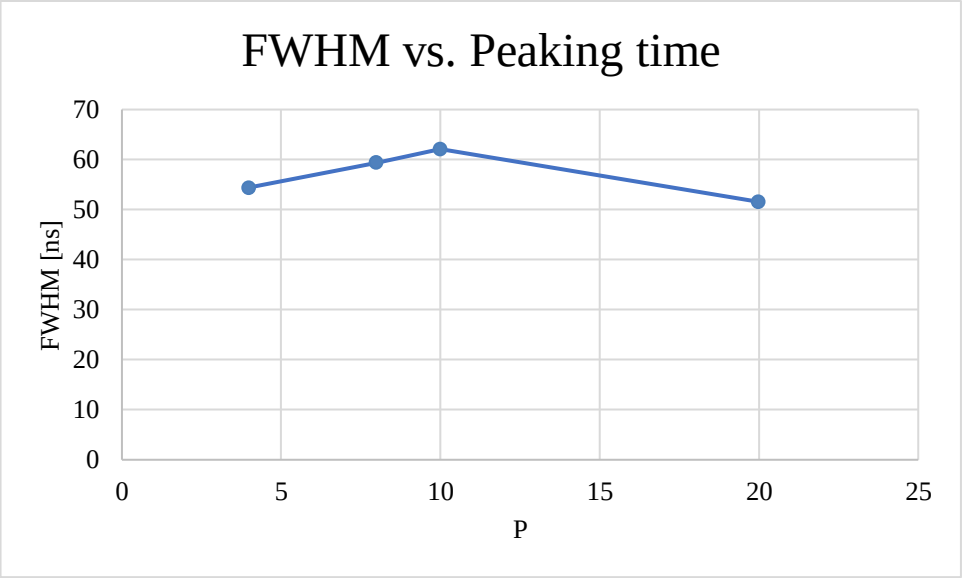

Figure 21: Time resolution at FWHM vs. Peaking time at G = 80 for HPGe and LYSO detectors.

For G = 80, the best time resolution is 51.55 ns at FWHM at P = 20.

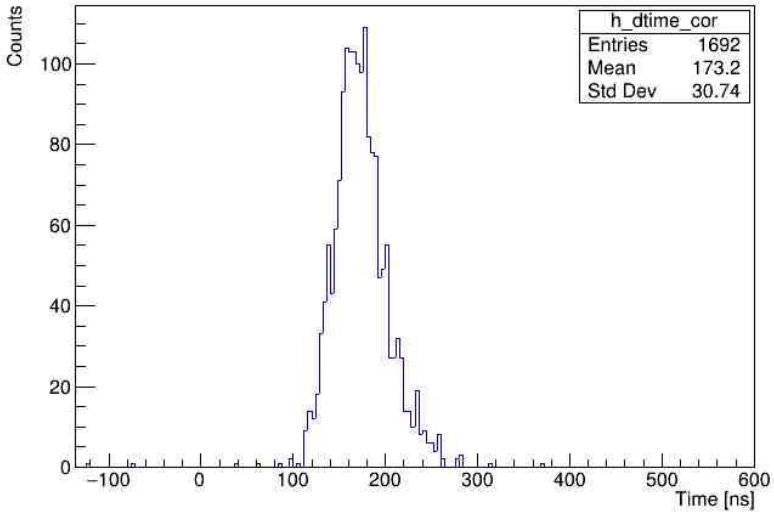

Figure 22: Time resolution for HPGe detector with P = 4 and G = 80.

6. DISCUSSION

The measured dead time matches that calculated from theory and falls in the lower end of the range. This dead time increases with sample length, as it did in the theory. In the dead time calculations, it is clear that as long as sample and event length are equal, the minimum dead time value is the same regardless of sample length. With a sample length of 100, the dead time fell very close to the minimum of 470 ns. But a sample length of 100 equals 400 ns, meaning that the dead time is now longer than the sample length. This made the measurement of the dead time difficult. For 500 and 1000, the dead time is also relatively small, and no longer larger than the sample length. These results will be relevant in case the entire waveform readout is necessary.

The figures above show the best results obtained for each case. Figure 10 and Figure 11 show the energy resolution for LYSO detectors. While the aim of this was not to finetune the settings to get the best resolution, the obtained resolution was of the same magnitude as that found in literature. In particular, changing the value of P may potentially lead to a good resolution for this type of detector.

Figure 12 shows the energy spectrum of ^{22}Na as obtained with a LYSO detector. This figure resembles Figure 4, since they were taken with similar scintillating detectors. This is because of the low-energy signals, which are due to Compton scattering in the crystal (Qin, et al., 2020).

Figure 13 and Figure 14 accurately show the effect of P and G, but these seem to saturate before the resolution we'd expect from literature are achieved. While this resolution is better than that from LYSO, as expected, it is also an order of magnitude larger than the expected resolution.

It should be noted that the values reported in the previous section are the smallest values; that is, the best resolution. However, these are not necessarily the optimal values. For example, in Figure 14 the best resolution is achieved at P = 100, but after P = 50, the gain in resolution is minimal. The improvement in resolution between P = 10 and P = 50 is slightly under 80%, while that between P = 50 and P = 60 is of 8%. Between P = 60 and P = 100, the improvement in resolution is just under 5%. So the optimal value of P may actually be 50, as this means less pileups. In non-optimal values of G, changes in P can produce improvements of over 90% (see appendix).

Comparison with Figure 13 shows that P has a bigger effect on energy resolution improvement than G. In this figure, the optimal G value increases resolution by less than 30%, a stark contrast from the 80% improvement offered by P.

Figure 15 and Figure 16 show the energy spectrum of ^{22}Na. These have the exact same settings except for the G and P values. These figures exemplify the importance of appropriate filter values. The noise is much larger in Figure 15. Moreover, the peak here has been split into two due to the higher energy data not being recorded due to an early cutoff. These peaks are akin to p_1 and p_2 from Figure 6. Figure 16 clearly has better resolution for the 511 keV peak. Furthermore, this figure shows two peaks; the first corresponds to the 511 keV peak from electron-positron annihilation, whereas the second corresponds to the 1275 keV peak.

In contrast, this second peak is not visible in Figure 15 or Figure 12. In Figure 15, this is because of the poorly chosen P and G values. In Figure 12 this has to do with the setup. Because of the way the LYSO scintillators are placed and the fact that the algorithm has been set up to look for coincidences, the photons produced by the deexcitation of the ^{22}Ne isotope are not detected. This is simply because these photons are emitted in all directions. Conversely, the annihilation photons are produced in pairs and in opposite directions and thus are easily detected by the scintillators. This is not an issue for the HPGe detector, so both peaks are visible in this case.

Figure 17 and Figure 18 show the time resolution of LYSO detectors. Like with the energy resolution, the aim of this measurement was not to get the best resolution. A minimum was not reached for G, hinting at the resolution improving with higher G. However, while the resolution is not close to that achieved in literature, which was in the order of picoseconds, the timing resolution is limited by the sampling rate of 250 MHz. Therefore, for this digitizer the timing resolution is as expected.

Figure 20 and Figure 21 show the time resolution achieved by an HPGe detector and a LYSO detector. This is resolution is not unlike the resolution expected from an HPGe detector, but by using elements like filters and by using a LYSO detector, this resolution should have been improved. In Figure 20, the resolution seemingly reaches a minimum at G = 20, but Figure 21 implies a saturation point was not reached. For the values studied, P seems to not have a large effect on the resolution. Better time resolution may imply going to P values that are unrealistic, as the pileups would become significant.

For both detectors, then, the time resolution is much worse than that found in literature. Figure 22 indicates that the implemented algorithm is not ideal. The tail visible on the right side is a result of pulses with a slow rise time. Figure 8 shows that the algorithm makes use of the falling edge instead of the rising edge. The rise time varies with event position, which shifts the fall time by a larger amount than the rise time (see appendix). Therefore, using the falling edge instead of the rising edge as a timestamp worsens the time resolution.

Moreover, the digitizer's software did not allow for separate settings for each channel. Therefore, in the setup for the time resolution of HPGE, both the HPGe and the LYSO detectors had to have the same settings. This was made to fit the HPGe detector, but perhaps better resolution could have been achieved had the settings also fit the LYSO detector.

Next to the flawed algorithm, other limitations of this research include the long time it took to process the events with the available technology, as well as limited access to the HPGe detector.

All this indicates that the resolution provided by the digitizer through the sole requirement of time and energy data is not good enough to meet the needs of nuclear data. Thus, a complete waveform readout will be necessary to achieve the desired resolution.

7. CONCLUSION

This research set out to test some technical specifications of the SIS3316 digitizer, specifically the dead time and time and energy resolution. Special attention was put on the viability of decreasing the data stored while still obtaining the necessary time and energy resolution with the digitizer. Dead time was measured by making use of random pulse generators. For the resolution studies, a ^{22}Na source was used, the activity of which was recorded by LYSO and an HPGe detectors. The available filtering and selective options were used to improve the resolution. From the obtained data, the resolution was calculated and compared to those obtained from literature.

The dead time was found to be within the theoretical dead time range, towards the lower end. Dead time was found to increase with increasing sample length. In contrast, it was found that, particularly for an HPGe detector, neither the time nor the energy resolution achieved were comparable to those found in literature. Only requiring energy and time data was not sufficient to achieve the required resolution; the entire waveform should be read out.

8. BIBLIOGRAPHY

Abuelhia, E., Alzimami, K., Alkhorayef, M., Podolyak, Z., & Spyrou, N. (2008). Measurement of coincidence timing resolution of scintillation detectors compared to semiconductor detectors to image three-photon positron annihilation. *Journal of radioanalytical and nuclear chemistry, 278*(3), 767-771.

Alkhorayef, M., Alzimami, K., Alfuraih, A., Alnafea, M., & Spyrou, N. M. (2012). Measurement of three gamma annihilation by lanthanum-based crystals compared with NaI(Tl) and HPGe. *Journal of Radioanalytical and Nuclear Chemistry, 291*(2), 493–496.

Alva-Sanchez, H., Zepeda-Barrios, A., Diaz-Martinez, V., Murrieta-Rodriguez, T., Martinez-Davalos, A., & Rodriguez-Villafuerte, M. (2018). Understanding the intrinsic radioactivity energy spectrum from 176 Lu in LYSO/LSO scintillation crystals. *Scientific reports, 8*(1), 1-7.

Auffray, E., Frisch, B., Geraci, F., Ghezzi, A., Gundacker, S., Hillemanns, H., . . . Pizzichemi, M. (2013). A comprehensive & systematic study of coincidence time resolution and light yield using scintillators of different size and wrapping. *IEEE Transactions on Nuclear Science, 60*(5), 3163-3171.

Bauer, M. W., Gylstorff, S., Madsen, E. B., & Mejlgaard, N. (2019). The Fukushima accident and public perceptions about nuclear power around the globe – a challenge & response model. *Environmental Communication, 13*(4), 505–526.

Beltrame, P., Bolle, E., Braem, A., Casella, C., Chesi, E., Clinthorne, N., . . . Weilhammer, P. (2011). Demonstration of an Axial PET concept for brain and small animal imaging. *Nuclear Instruments and Methods in Physics Research Section A: Accelerators, Spectrometers, Detectors and Associated Equipment, 628*(1), 426-429.

Boromiza, M., Borcea, C., Dessagne, P., Ghita, D., Glodariu, T., Henning, G., . . . Turturica, G. (2020). Nucleon inelastic scattering cross sections on O 16 and Si 28. *Physical Review C, 101*(2), 024604.

Crespi, F. C., Vandone, V., Brambilla, S., Camera, F., Million, B., Riboldi, S., & Wieland, O. (2010). HPGe detectors timing using pulse shape analysis techniques. *Nuclear Instruments and Methods in Physics Research Section A: Accelerators, Spectrometers, Detectors and Associated Equipment, 620*(2-3), 299-304.

Daube-Witherspoon, M. E. (2014). Generic Performance Measures. In D. L. Bailey, H. J. L, A. Todd-Pokropek, & A. van Aswegen, *Nuclear Medicine Physics: A Handbook for Teachers and Students.* Vienna: Intenational Atomic Energy Agency.

Doroud, K., Williams, M. C., Zichichi, A., & Zuyeuski, R. (2015). Comparative timing measurements of LYSO and LFS-3 to achieve the best time resolution for TOF-PET. *Nuclear Instruments and Methods in Physics Research Section A: Accelerators, Spectrometers, Detectors and Associated Equipment, 793*, 57-61.

European Commission. (2020, June 04). *The JRC Neutron Time-of-Flight Facility*. Retrieved from European Commission: https://ec.europa.eu/jrc/en/research-facility/linear-electron-accelerator-facility

Gladen, R. W., Chirayath, V. A., Fairchild, A. J., Manry, M. T., Koymen, A. R., & Weiss, A. H. (2020). Efficient machine learning approach for optimizing the timing resolution of a high purity germanium detector. *Nuclear Instruments and Methods in Physics*

Research Section A: Accelerators, Spectrometers, Detectors and Associated Equipment, 981, 164505.

IAEA. (2021). *Live Chart of Nuclides*. Retrieved from IAEA: https://www-nds.iaea.org/relnsd/vcharthtml/VChartHTML.html

Jun-Hui, L., Jin-Xing, C., Jiong-Hui, X., Feng-Feng, C., Dao-Wu, L., Zhi-Ming, Z., . . . Long, W. (2015). Investigation of the time performance of a LYSO array for TOF-PET. *Chinese Physics C, 39*(12), 128201.

Kerveno, M., Bacquias, A., Borcea, C., Dessagne, P., Henning, G., Mihailescu, L. C., . . . Thiry, J. C. (2015). From γ emissions to (n, xn) cross sections of interest: The role of GAINS and GRAPhEME in nuclear reaction modeling. *The European Physical Journal A, 51*(12), 1-18.

Kramar, U. (2017). *Encyclopedia of Spectroscopy and Spectrometry.* (J. C. Lindon, G. E. Tranter, & D. W. Koppenaal, Eds.) Academic Press.

Lecoq, P. (2020). Scintillation Detectors for Charged Particles and Photons. In C. Fabjan, & H. Schopper, *Particle Physics Reference Library.* Springer.

Lee, M., Lee, D., Ko, E., Park, K., Kim, J., Ko, K., . . . Cho, G. (2020). Pulse pileup correction method for gamma-ray spectroscopy in high radiation fields. *Nuclear Engineering and Technology, 52*(5), 1029-1035.

Luo, X. L., Modamio, V., Nyberg, J., Valiente-Dobón, J. J., Nishada, Q., De Angelis, G., . . . Wadsworth, R. (2018). Pulse pile-up identification and reconstruction for liquid scintillator based neutron detectors. *Nuclear Instruments and Methods in Physics Research Section A: Accelerators, Spectrometers, Detectors and Associated Equipment, 897*, 59-65.

Lutz, G., & Klanner, R. (2020). Solid State Detectors . In C. Fabjan, & H. Schopper, *Particle Physics Reference Library.* Springer.

Mihailescu, L. C., Borcea, C., & Plompen, A. J. (2007). Data acquisition with a fast digitizer for large volume HPGe detectors. *Nuclear Instruments and Methods in Physics Research Section A: Accelerators, Spectrometers, Detectors and Associated Equipment, 578*(1), 298-305.

Mihailescu, L., Olah, L., Borcea, C., & Plompen, A. (2004). A new HPGe setup at Gelina for measurement of gamma-ray production cross-sections from inelastic neutron scattering. *Nuclear Instruments and Methods in Physics Research Section A: Accelerators, Spectrometers, Detectors and Associated Equipment, 531*(3), 375–391.

Moszynski, M., Kapusta, M., Nassalski, A., Szczesniak, T., Wolski, D., Eriksson, L., & Melcher, C. L. (2006). New prospects for time-of-flight PET with LSO scintillators. *IEEE Transactions on Nuclear Science, 53*(5), 2484-2488.

Negret, A., Borcea, C., Drohe, J., Mihailescu, L. C., Plompen, A., & Wynants, R. (2007). A new setup for neutron inelastic cross section measurements. *International Conference on Nuclear Data for Science and Technology* (pp. 1015–1018). EDP Sciences.

Pirovano, E., Beyer, R., Junghans, A., Nolte, R., Nyman, M., & Plompen, A. (2017). Measurements of neutron scattering angular distributions with a new scintillator setup. *EPJ Web of Conferences. 146*, p. 11008. EDP Sciences.

Qin, J., Lai, C., Xiao, J., Lu, X., Zhu, T., Liu, R., & Ye, B. (2020). Characteristics and time resolutions of two CeBr3 gamma-ray spectrometers. *Radiation Detection Technology and Methods, 4*(3), 327-336.

Rouki, C. A. (2012). High resolution measurement of neutron inelastic scattering cross-sections for 23Na. *Nuclear Instruments and Methods in Physics Research Section A: Accelerators, Spectrometers, Detectors and Associated Equipment, 672*, 82–93.

SIS GmbH. (2020). *SIS3316 16 Channel VME Digitizer: User Manual.* Hamburg: SIS GmbH.

van Eijk, C. W. (2014). Basic Radiation Detectors. In D. L. Bailey, J. L. Humm, A. Todd-Pokropek, v. Aswegen, & A, *Nuclear Medicine Physics: A Handbook for Teachers and Students.* Vienna: International Atomic Energy Agency.

Zahn, G. S., Ribeiro Jr, I. S., & Genezini, F. A. (2019). Pile-up correction for coincidence counting using a CAEN 1724 digitizer. . *Brazilian Journal of Radiation Sciences, 7*(2A).

Zhao, J. W., Sun, B. H., Tanihata, I., Terashima, S., Zhu, L. H., Enomoto, A., . . . Takeuchi, Y. (2016). Reaching time resolution of less than 10 ps with plastic scintillation detectors. *Nuclear Instruments and Methods in Physics Research Section A: Accelerators, Spectrometers, Detectors and Associated Equipment, 823*, 41 - 46.

9. APPENDIX

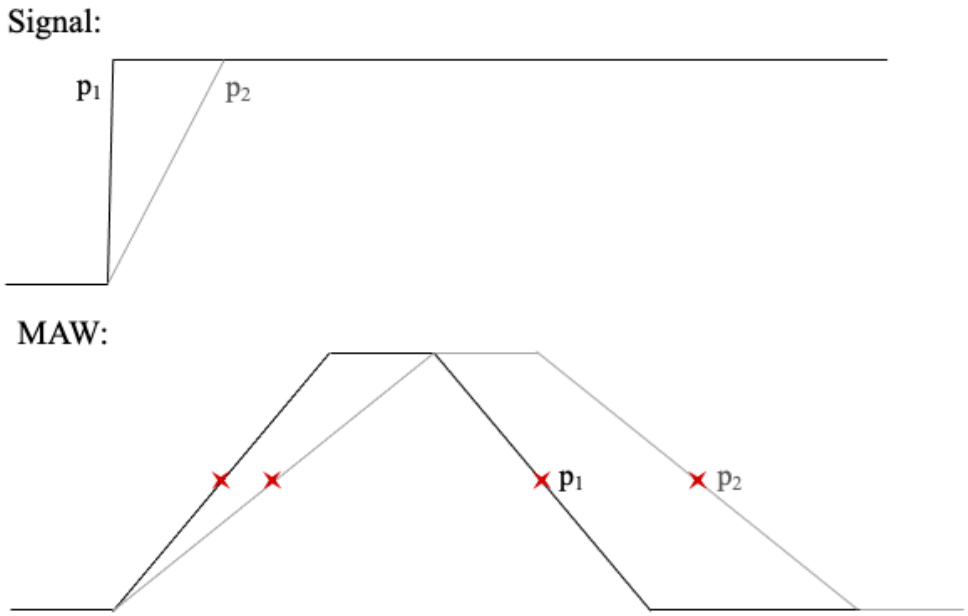

Figure 23: MAW for signals with different rise times and its effect on time resolution. The red crosses represent the timestamps at 50% maximum on their rising and falling edges.

1. Energy resolution for a LYSO detector

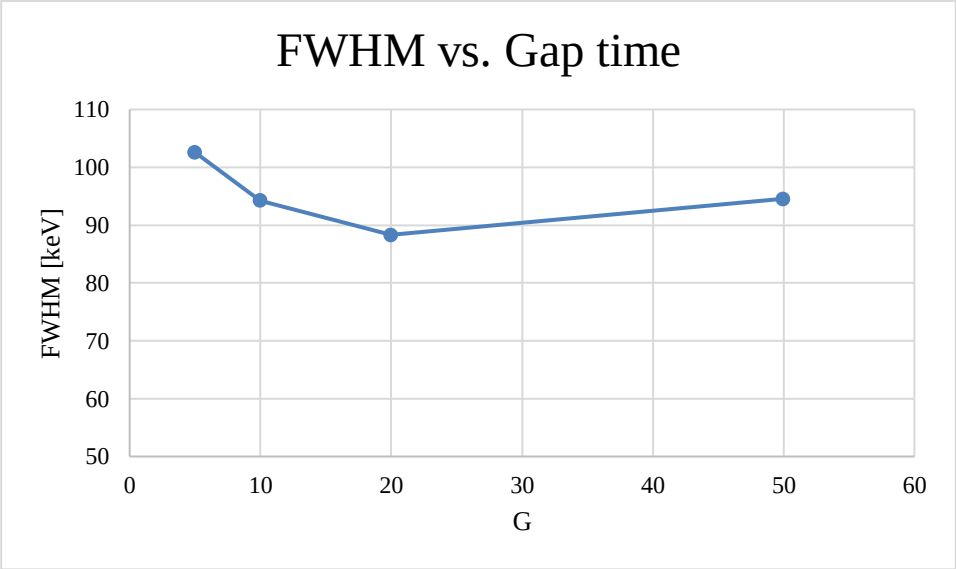

Figure 24: Energy resolution at FWHM for the 511 keV peak vs. Gap time with P = 50 for a LYSO detector.

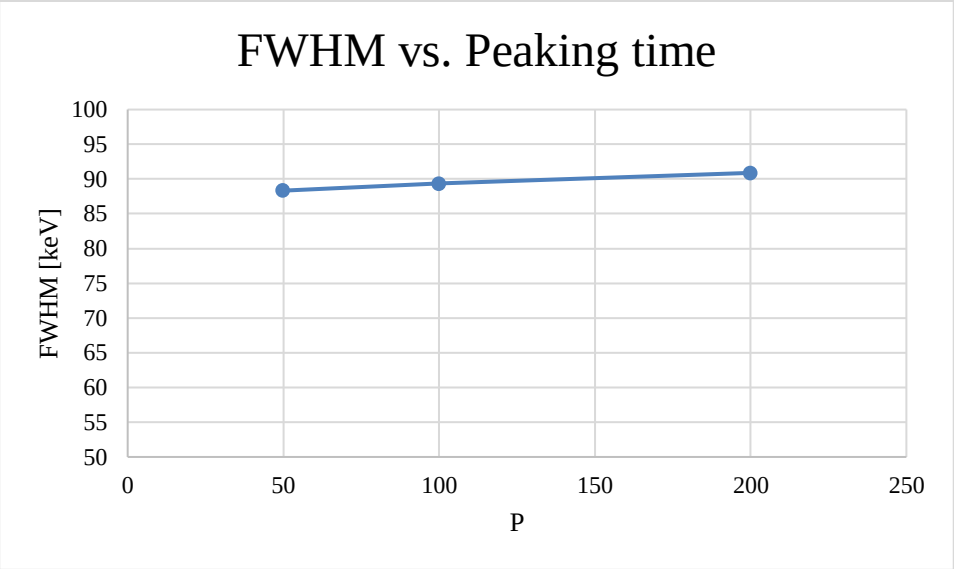

Figure 25: Energy resolution at FWHM for the 511 keV peak vs. Peaking time with G = 20 for a LYSO detector.

These correspond to the energy resolution achieved by the second LYSO detector.

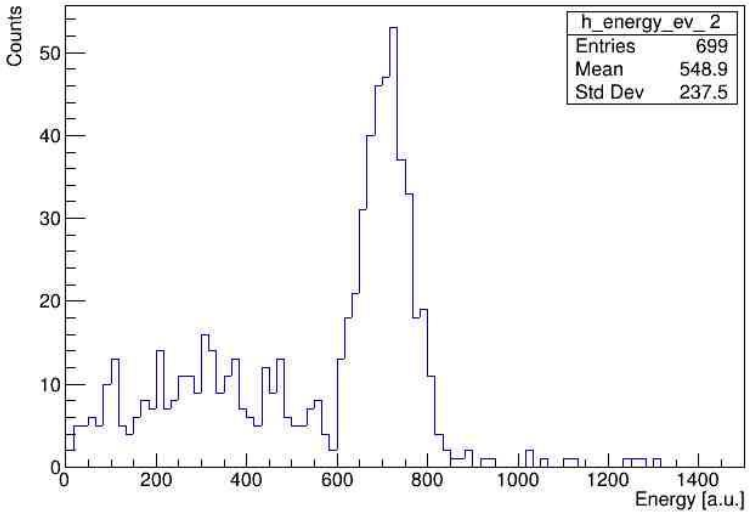

Figure 26: Energy spectrum for ^{22}Na with G = 5 and P = 50 with LYSO detectors. This was the worst energy resolution achieved with the second detector.

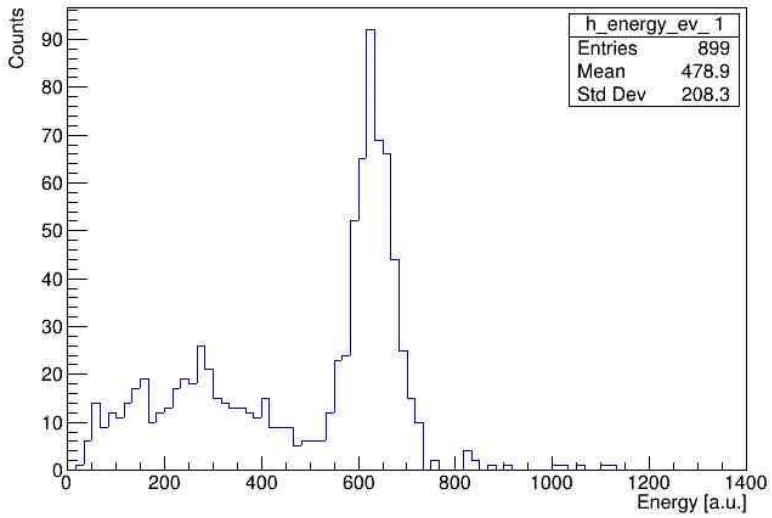

Figure 27: Energy spectrum for ^{22}Na with G = 10 and P = 50 with LYSO detectors. This was the worst energy resolution achieved with the first detector.

2. Preliminary energy resolution for HPGe and LYSO detectors

2.1 LYSO detector

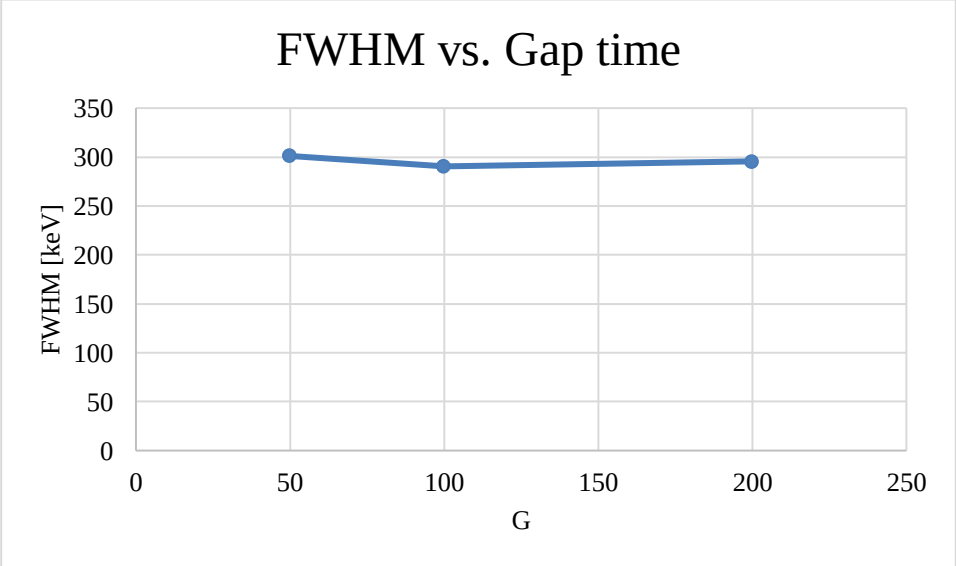

Figure 28: Preliminary energy resolution at FWHM for the 511 keV peak vs. Gap time with P = 50 for a LYSO detector.

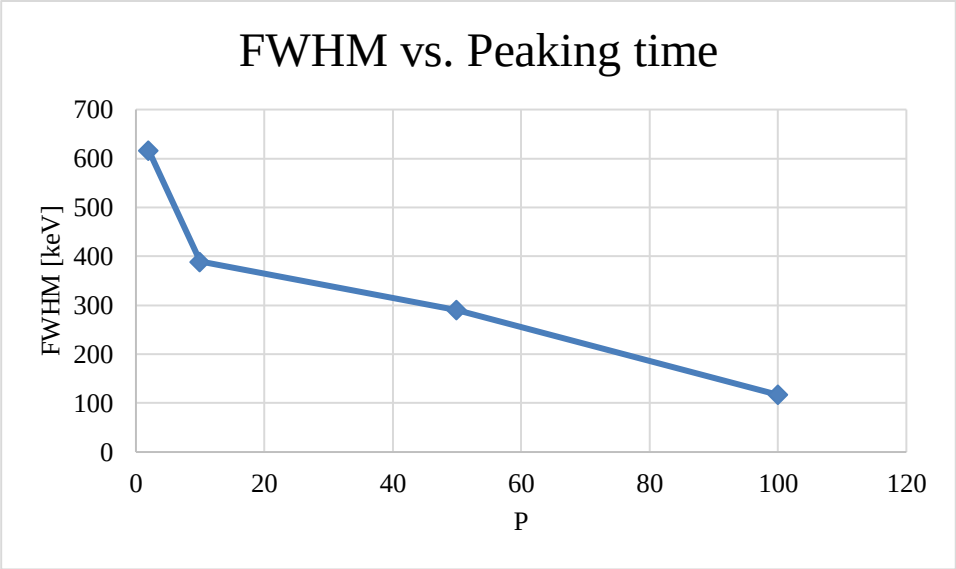

Figure 29: Preliminary energy resolution at FWHM for the 511 keV peak vs. Peaking time with G = 100 for a LYSO detector.

2.2 HPGE detector

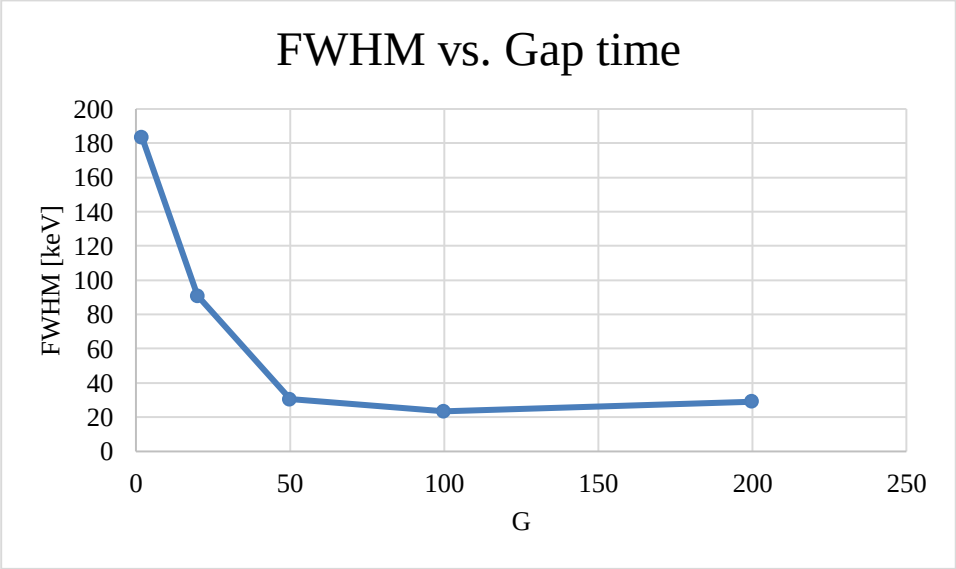

Figure 30: Preliminary energy resolution at FWHM for the 511 keV peak vs. Gap time with P = 50 for an HPGe detector.

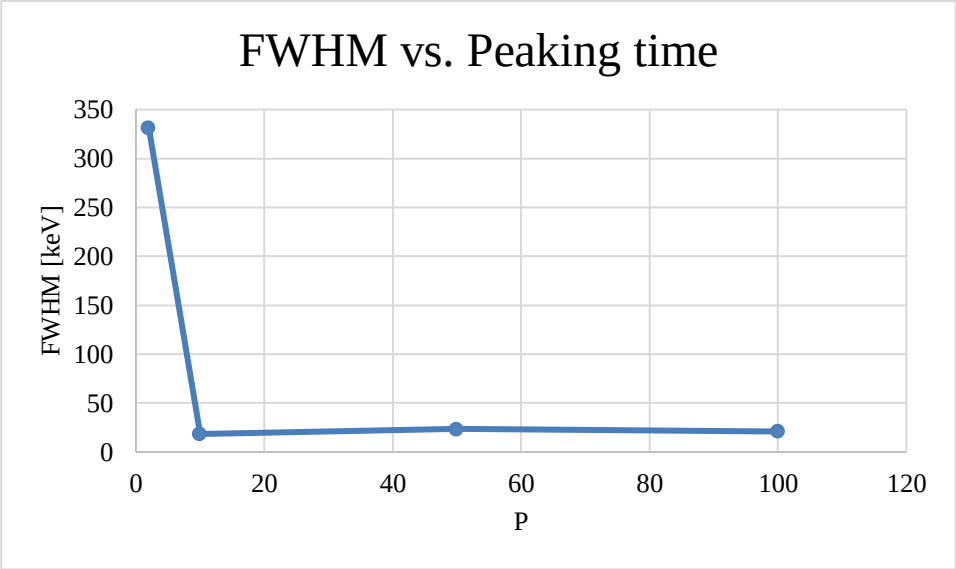

Figure 31: Preliminary energy resolution at FWHM for the 511 keV peak vs. Peaking time with G = 100 for an HPGe detector.

Here, the settings were chosen such that a compromise was reached between the most suitable settings for the HPGe detector and those for the LYSO detector. These also include less events than the non-preliminary data.

3. Energy resolution for a HPGe detector

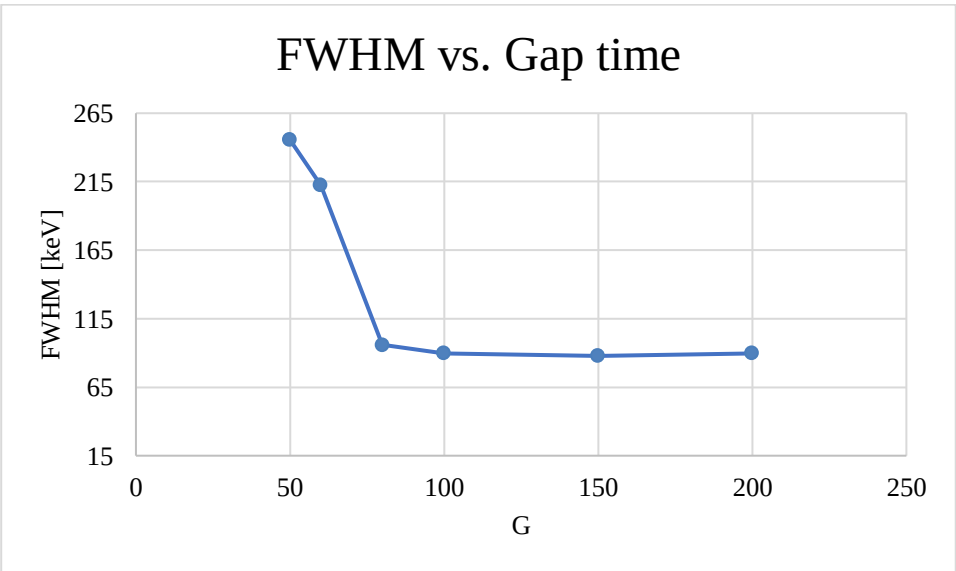

Figure 32: Energy resolution at FWHM for the 511 keV peak vs. Gap time with P = 10 for an HPGe detector.

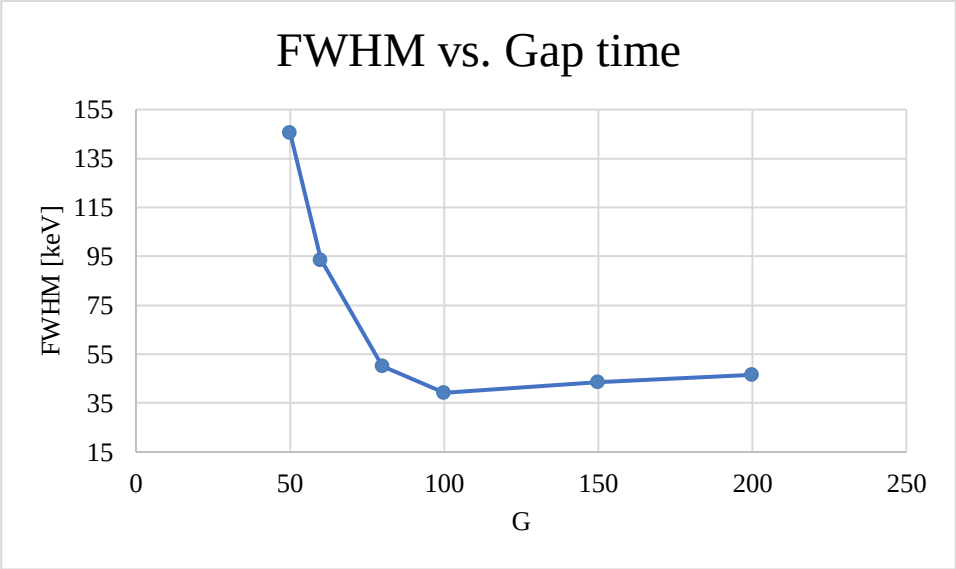

Figure 33: Energy resolution at FWHM for the 511 keV peak vs. Gap time with P = 20 for an HPGe detector.

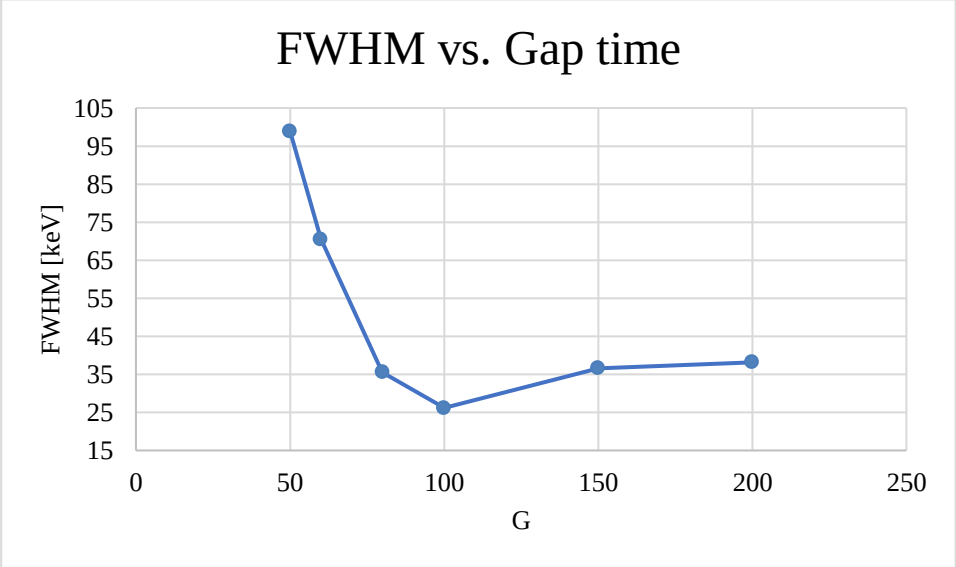

Figure 34: Energy resolution at FWHM for the 511 keV peak vs. Gap time with P = 30 for an HPGe detector.

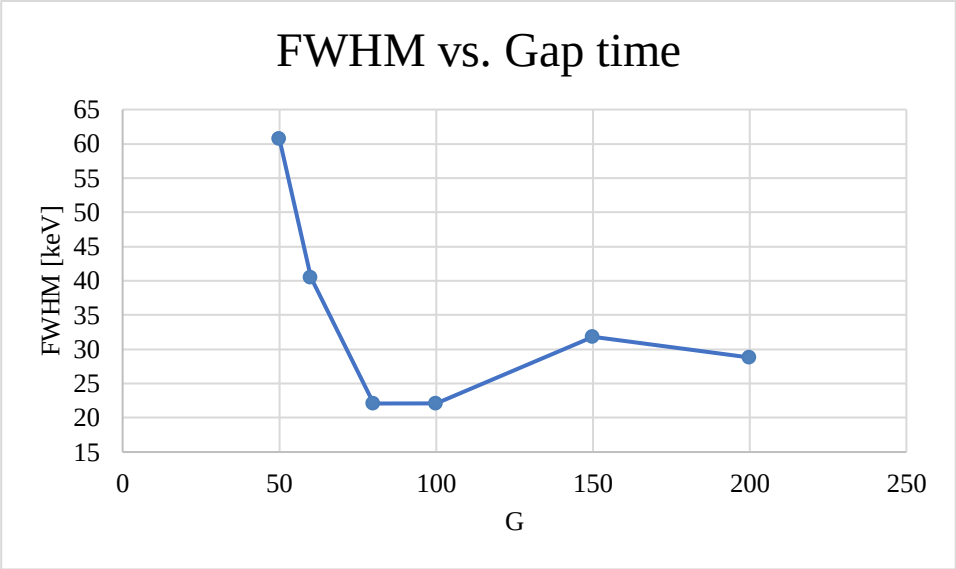

Figure 35: Energy resolution at FWHM for the 511 keV peak vs. Gap time with P = 50 for an HPGe detector.

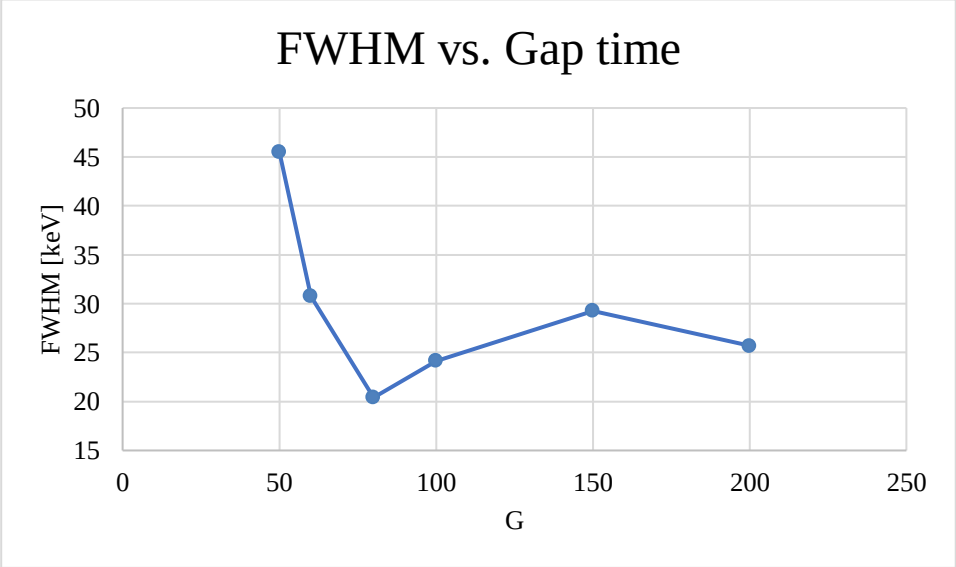

Figure 36: Energy resolution at FWHM for the 511 keV peak vs. Gap time with P = 60 for an HPGe detector.

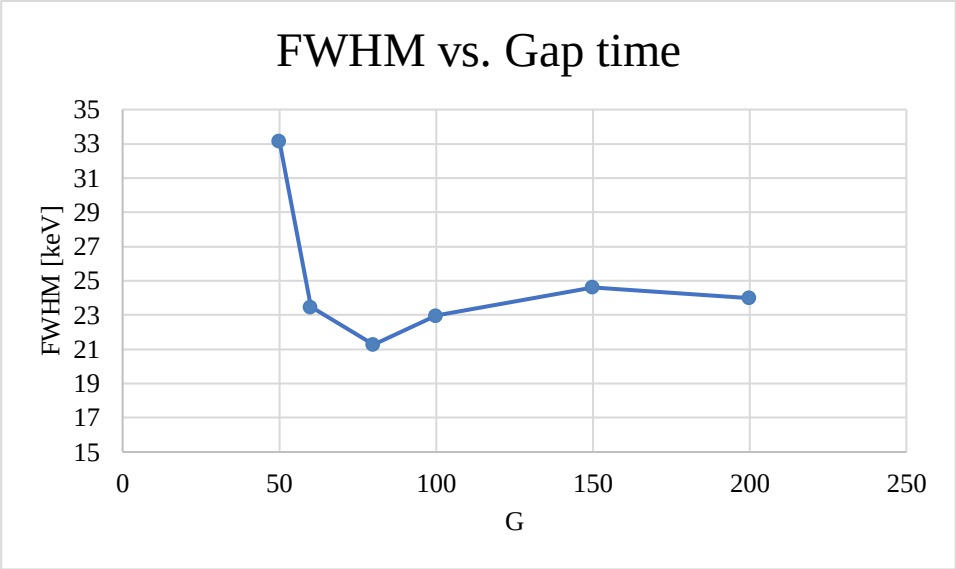

Figure 37: Energy resolution at FWHM for the 511 keV peak vs. Gap time with P = 80 for an HPGe detector.

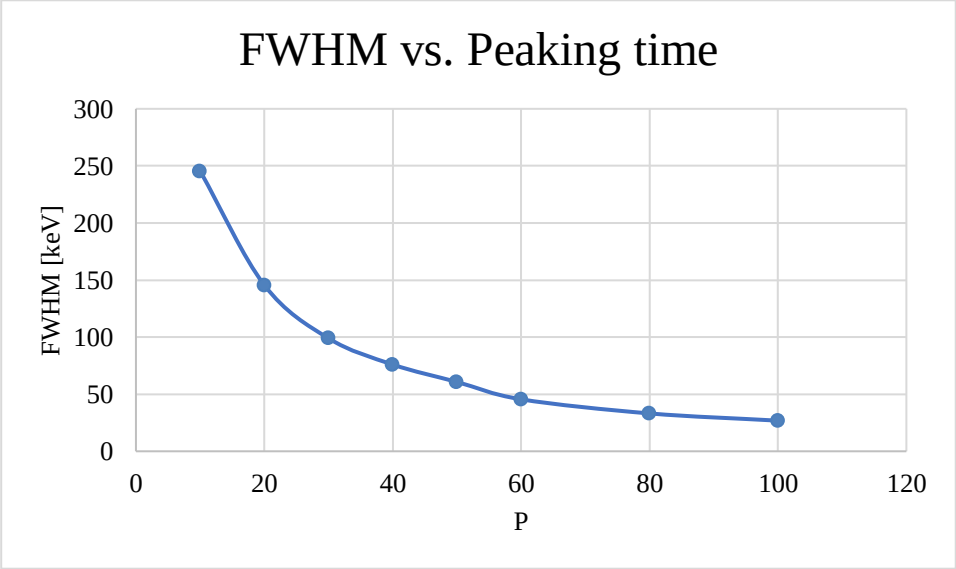

Figure 38: Energy resolution at FWHM for the 511 keV peak vs. Peaking time with G = 50 for an HPGe detector.

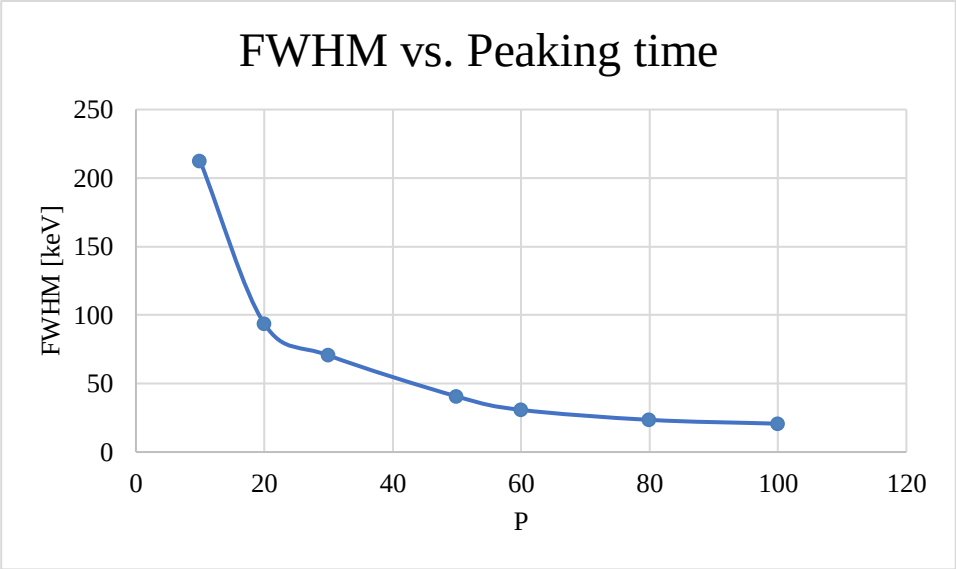

Figure 39: Energy resolution at FWHM for the 511 keV peak vs. Peaking time with G = 60 for an HPGe detector.

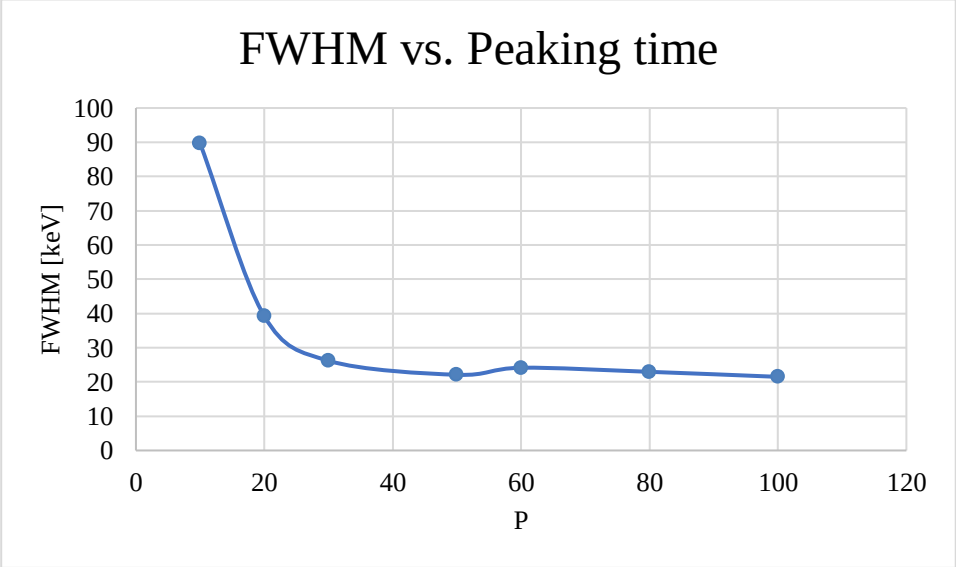

Figure 40: Energy resolution at FWHM for the 511 keV peak vs. Peaking time with G = 100 for an HPGe detector.

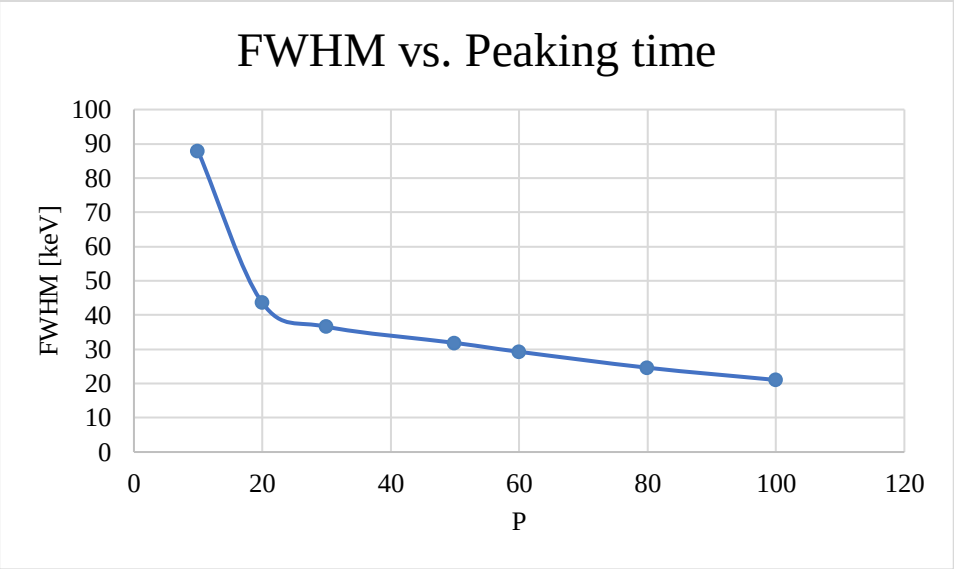

Figure 41: Energy resolution at FWHM for the 511 keV peak vs. Peaking time with G = 150 for an HPGe detector.

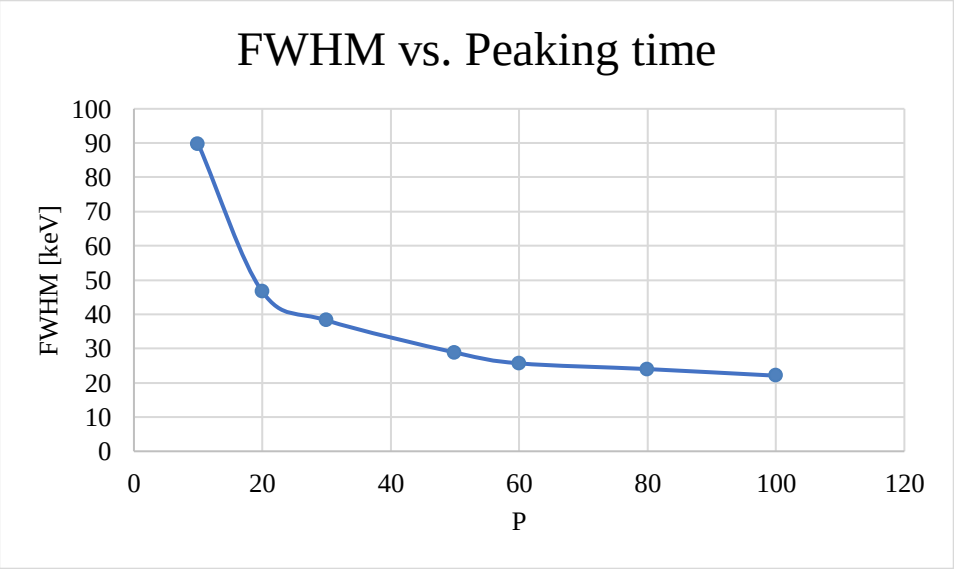

Figure 42: Energy resolution at FWHM for the 511 keV peak vs. Peaking time with G = 200 for an HPGe detector.

4. Time resolution for LYSO detectors

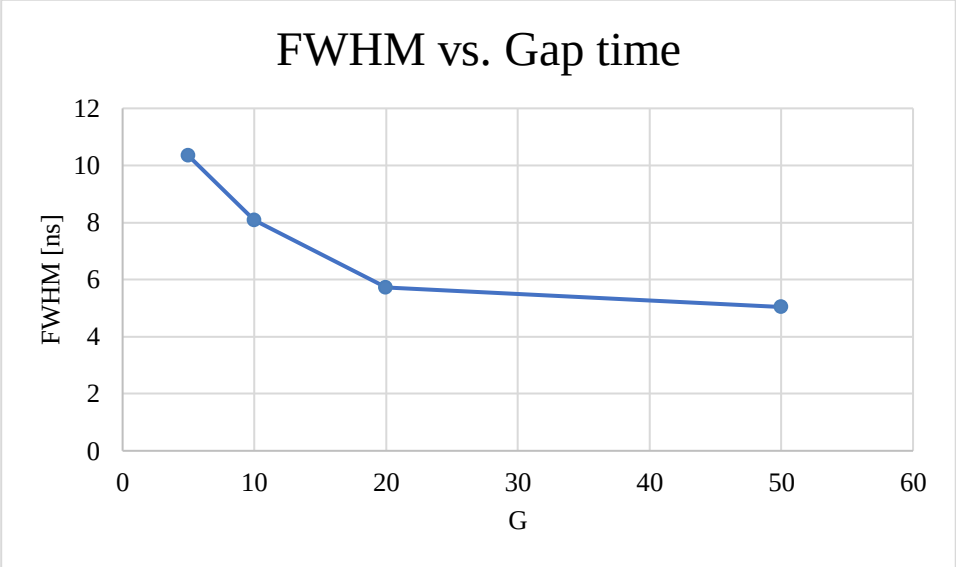

Figure 43: Time resolution at FWHM vs. Gap time at P = 4 for LYSO detectors.

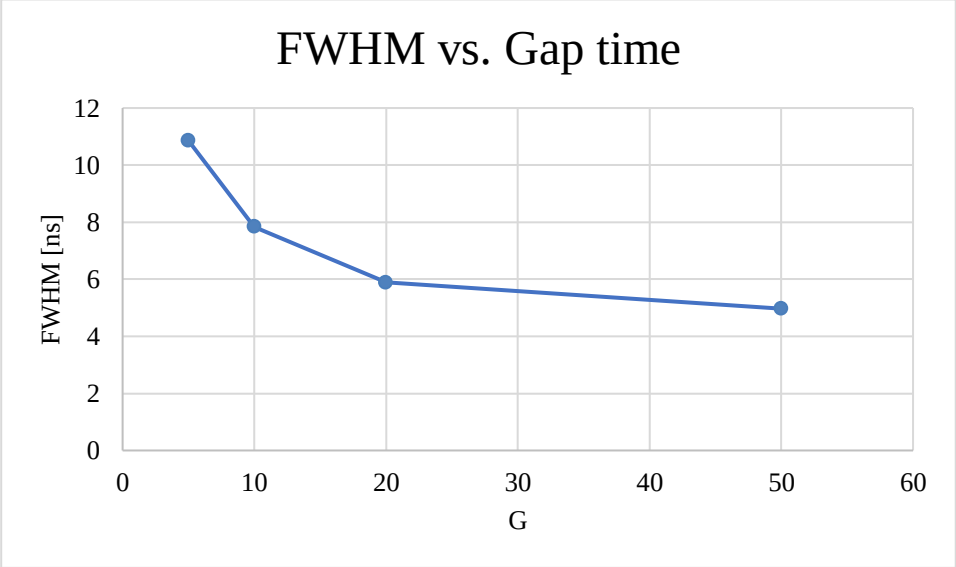

Figure 44: Time resolution at FWHM vs. Gap time at P = 4 for LYSO detectors.

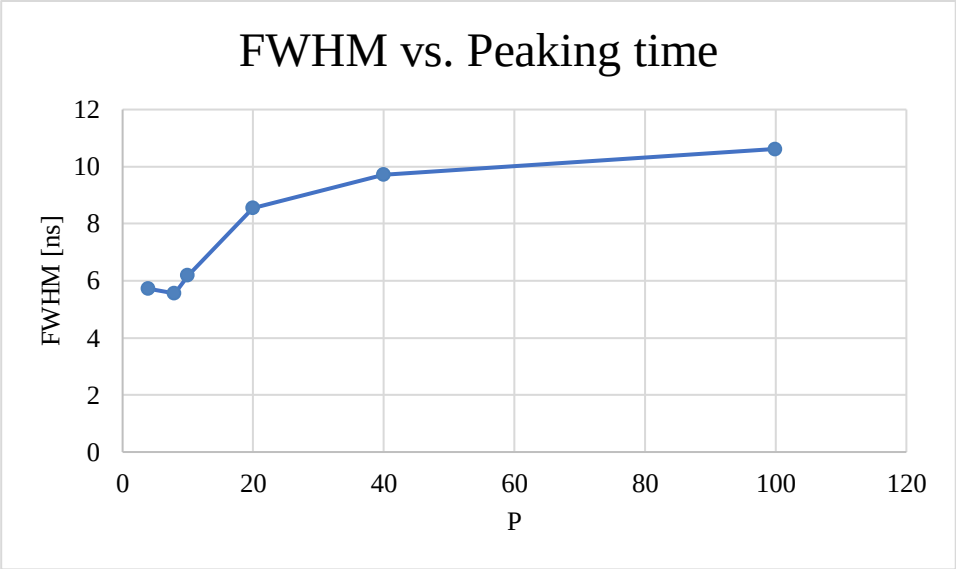

Figure 45: Time resolution at FWHM vs. Peaking time at G = 20 for LYSO detectors.

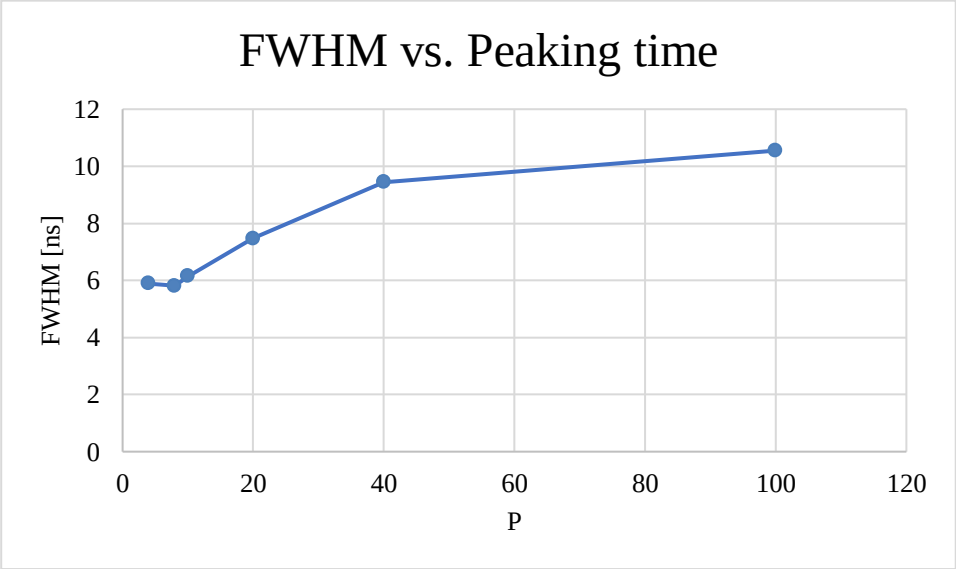

Figure 46: Time resolution at FWHM vs. Peaking time at G = 20 for LYSO detectors.

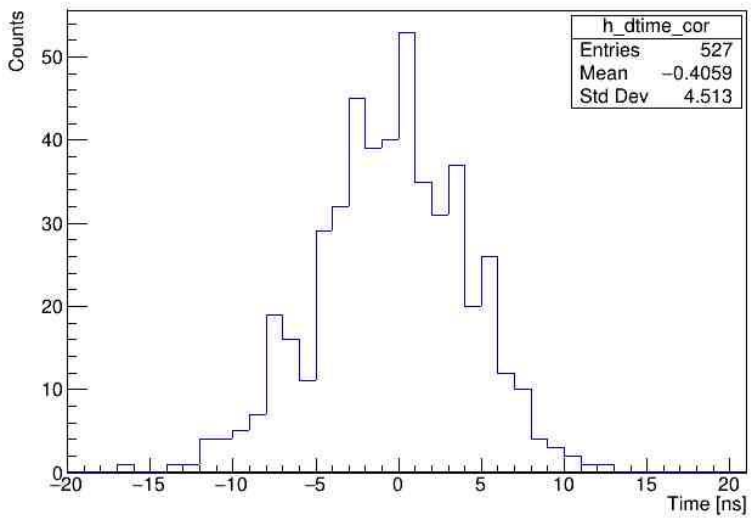

Figure 47: Time resolution for LYSO detectors with P = 4 and G = 5. This was the worst time resolution obtained for this setup.

5. Time resolution for HPGe and LYSO detectors

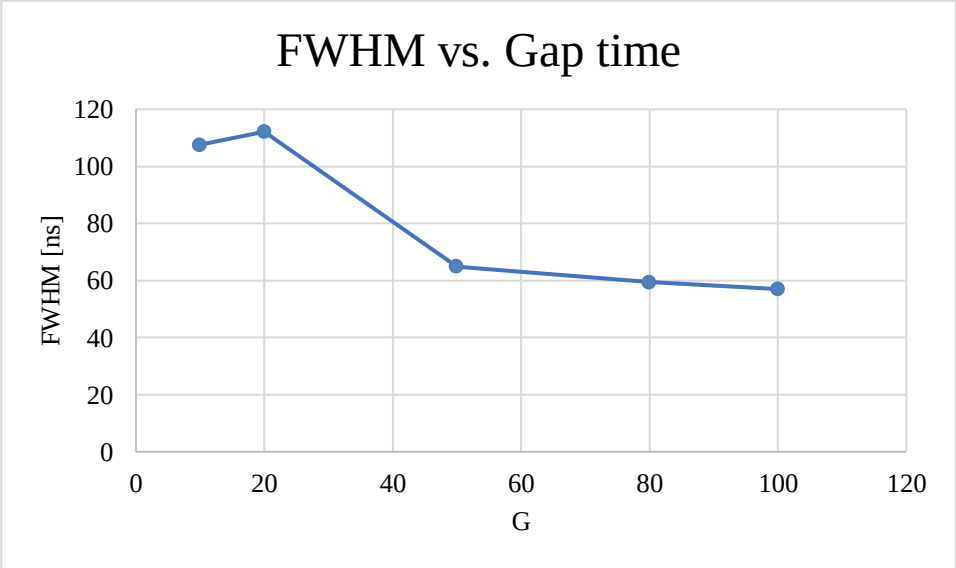

Figure 48: Time resolution at FWHM vs. Gap time at P = 8 for HPGe and LYSO detectors.

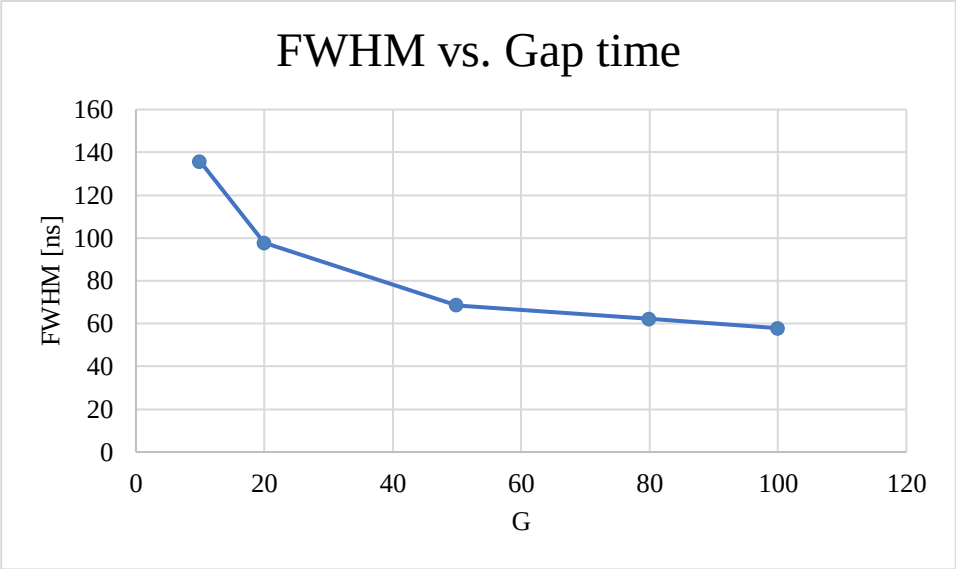

Figure 49: Time resolution at FWHM vs. Gap time at P = 10 for HPGe and LYSO detectors.

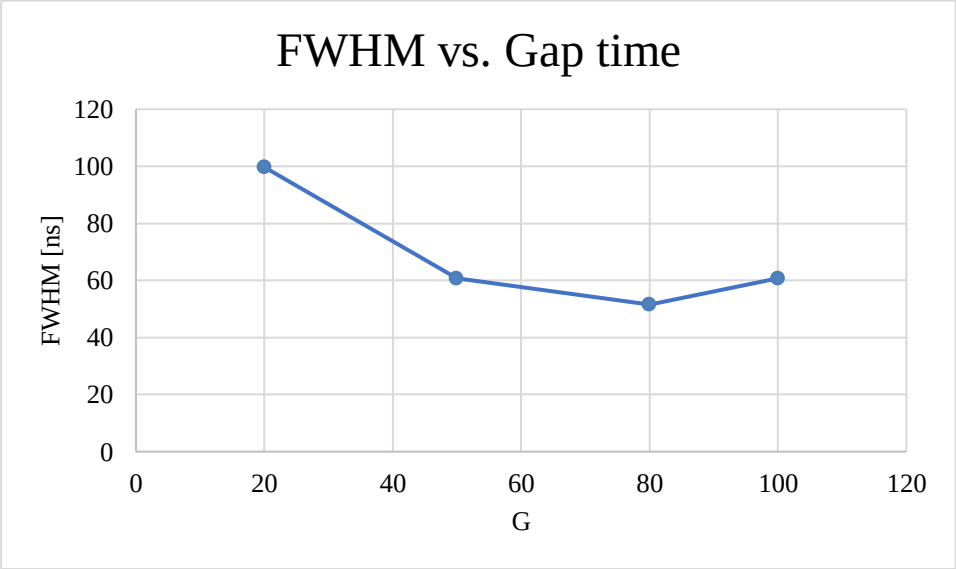

Figure 50: Time resolution at FWHM vs. Gap time at P = 20 for HPGe and LYSO detectors.

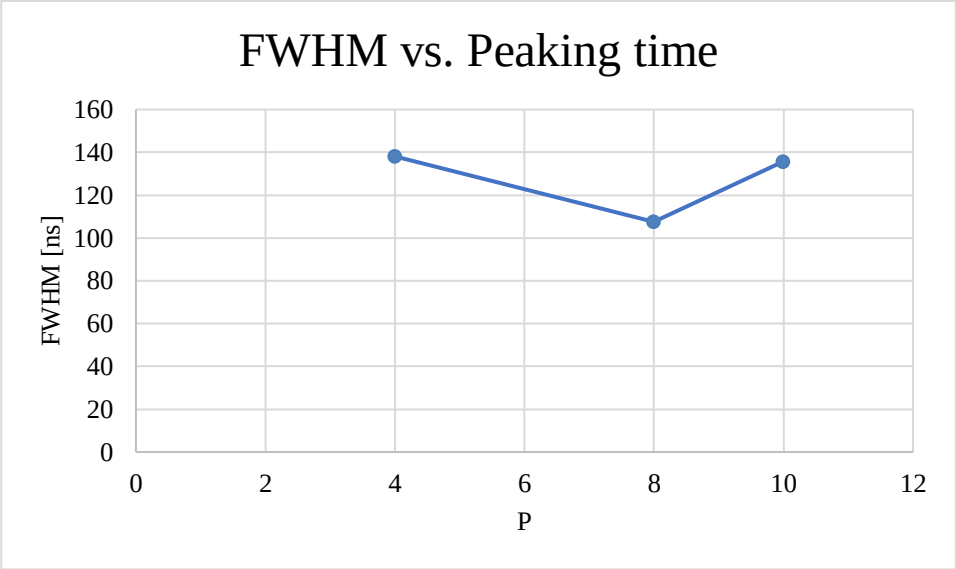

Figure 51: Time resolution at FWHM vs. Peaking time at G = 10 for HPGe and LYSO detectors.

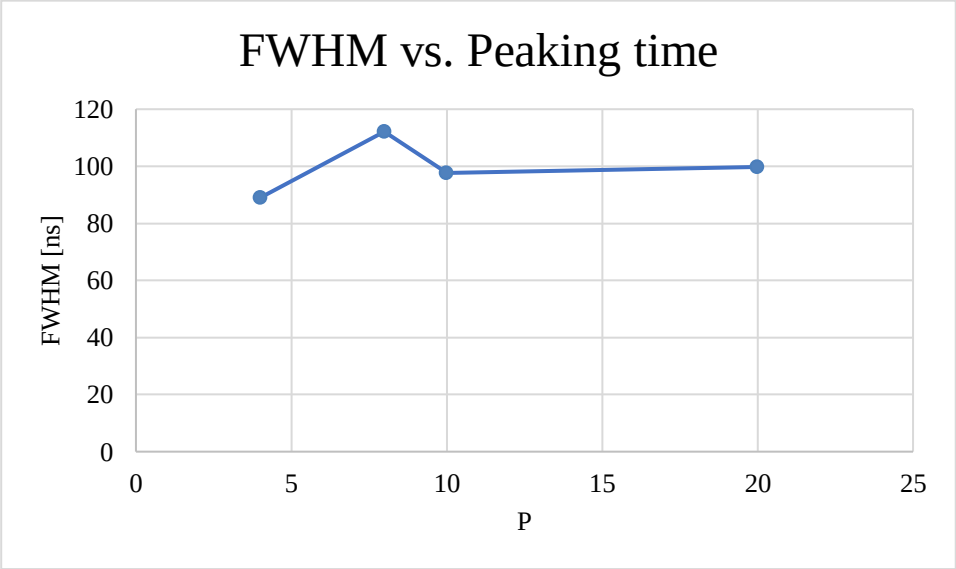

Figure 52 Time resolution at FWHM vs. Peaking time at G = 20 for HPGe and LYSO detectors.

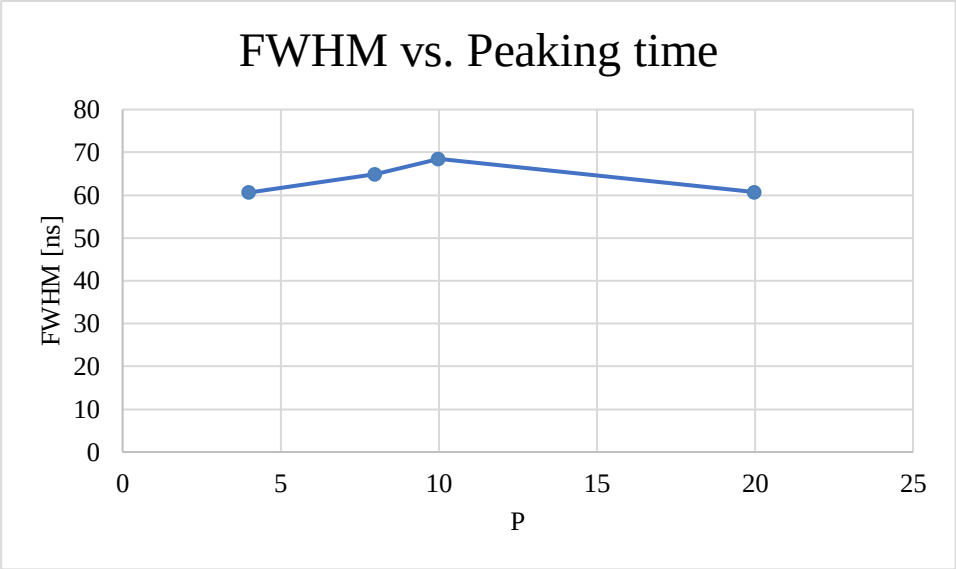

Figure 53: Time resolution at FWHM vs. Peaking time at G = 50 for HPGe and LYSO detectors.

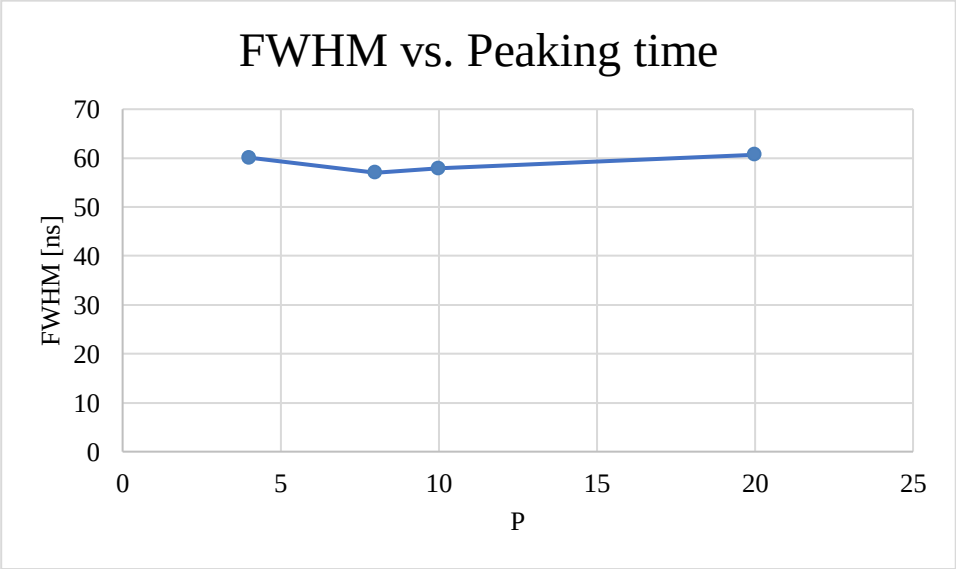

Figure 54: Time resolution at FWHM vs. Peaking time at G = 100 for HPGe and LYSO detectors.

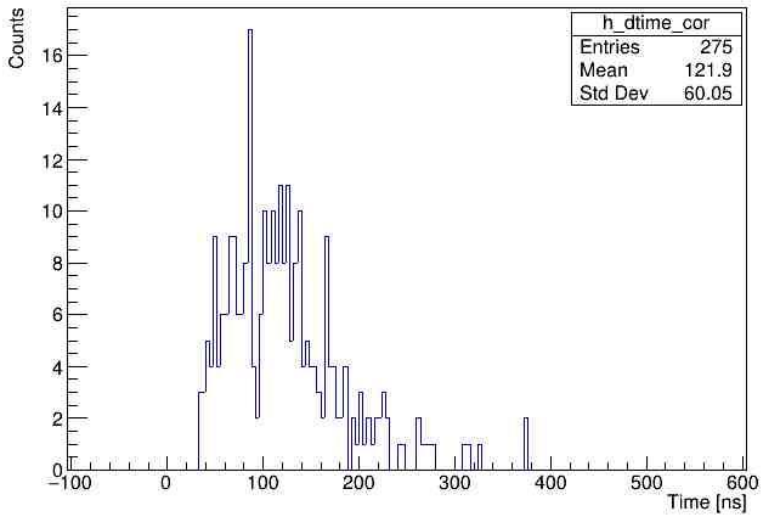

Figure 55: Time resolution for HPGe detector with P = 4 and G = 10. This was the worst time resolution achieved for this setup.